All ETDs from UAB

UAB Theses & Dissertations

1993

Application of a laser beam profile reshaper to enhance performance of holographic projection systems.

Wu Jiang

INFORMATION TO USERS

This manuscript has been reproduced from the microfilm master. UMI films the text directly from the original or copy submitted. Thus, some thesis and dissertation copies are in typewriter face, while others may be from any type of computer printer.

The quality of this reproduction is dependent upon the quality of the copy submitted. Broken or indistinct print, colored or poor quality illustrations and photographs, print bleedthrough, substandard margins, and improper alignment can adversely affect reproduction.

In the unlikely event that the author did not send UMI a complete manuscript and there are missing pages, these will be noted. Also, if unauthorized copyright material had to be removed, a note will indicate the deletion.

Oversize materials (e.g., maps, drawings, charts) are reproduced by sectioning the original, beginning at the upper left-hand corner and continuing from left to right in equal sections with small overlaps. Each original is also photographed in one exposure and is included in reduced form at the back of the book.

Photographs included in the original manuscript have been reproduced xerographically in this copy. Higher quality 6" x 9" black and white photographic prints are available for any photographs or illustrations appearing in this copy for an additional charge. Contact UMI directly to order.

.

Order Number 9419291

Application of a laser beam profile reshaper to enhance performance of holographic projection systems

Jiang, Wu, Ph.D.

University of Alabama at Birmingham, 1993

U·M·I

APPLICATION OF A LASER BEAM PROFILE RESHAPER
TO ENHANCE PERFORMANCE OF HOLOGRAPHIC
PROJECTION SYSTEMS

by

WU JIANG

A DISSERTATION

Submitted in partial fulfillment of the requirements for the degree of
Doctor of Philosophy in the Department of Physics
in the Graduate School, The University of
Alabama at Birmingham

BIRMINGHAM, ALABAMA

1993

ABSTRACT OF DISSERTATION
GRADUATE SCHOOL, UNIVERSITY OF ALABAMA AT BIRMINGHAM

Degree ___Doctor of Philosophy___ Major Subject ___Physics___

Name of Candidate ___Wu Jiang___

Title ___Application of a laser beam profile reshaper
to enhance performance of holographic projection systems___

Since many illumination applications, such as holographic projection systems, material processing, and laser fusion, require a laser beam to have a uniform energy profile, it is very important to provide a simple and energy efficient beam profile reshaping system. This study evaluates a refractive beam profile reshaping system and its application to a holographic projection system. This reshaper is a two-plano-aspherical lens system which can be designed to convert effectively an arbitrary radially symmetric beam profile into a desired beam profile. In this study, a Gaussian beam profile of a Helium Cadmium laser is converted into a uniform beam profile. The optical design of this reshaping system was based on two conditions: conservation of energy and constant optical path length, by which differential equations were written to solve the shapes of the two aspherical surfaces of the reshaper. The optical performance of this system was analyzed by the flux-flow equation and conventional optical analysis software (GENII-PLUS). Experimental results of testing this reshaper demonstrated that such a two-aspherical-lens system is an energy efficient and simple beam profile reshaping system. Therefore, the design theory has been established. Experimental results also have established that a reshaper designed to operate at one wavelength can effectively reshape a laser beam of a different wavelength, provided the lens spacing of the reshaper is adjusted to compensate for the change in index of the lens associated with the change in wavelength. Acceptable assembly tolerances were also investigated by

ii

tilting and decentering the two lenses, and the test results illustrated that such a two-lens reshaping system is a very stable system. This reshaper was then integrated into a holographic projection system which produces multiple coherent, uniform irradiance beams to generate various interference patterns. Based on the performance of the prototype of the laser beam reshaper and the holographic projector, a UV laser reshaping system was designed. It will be used in a UV holographic projector which will produce directional light filters, optical arrays, and other micro-elements.

The design and testing of the refractive beam reshaping system and its application to the holographic system demonstrated that such a two-lens reshaping system provides a simple and efficient solution to many uniform illumination applications.

Abstract Approved by: Committee Chairman _____

Program Director _____

Date _____ Dean of Graduate School _____

iii

DEDICATION

To my parents, who sacrificed everything to raise three children during the most difficult time of our family and our nation. My foremost goal is to make them proud.

献给我敬爱的父母

春夜喜雨

杜 甫

好雨知时节，当春乃发生。
随风潜入夜，润物细无声。
野径云俱黑，江船火独明。
晓看红湿处，花重锦官城。

ACKNOWLEDGEMENTS

I wish to express my appreciation to each of the members of my graduate committee, Dr. Christer Bennewitz, Dr. Joseph G. Harrison, Dr. James C. Martin, Dr. Bill Rosenblum, Dr. David L. Shealy, and Dr. John H. Young, for their support and encouragement during my work on this project. I also wish to express my gratitude to Mr. Ken Baker of Optimerix, Inc., Van Nuys, California, for supporting this enjoyable research project.

The 4 years of graduate study in the Department of Physics of UAB has been a memorable experience. Dr. David Shealy, my advisor, guided and encouraged me to become an independent scientist. I learned hard work from him by reading e-mail he sent at 3:00 am; I also learned desire for excellence from him by revising a paper four or five times before submitting it. (The 4 years working for you have been very enjoyable. Thank you.) I also would like to thank Dr. David Agresti, Dr. Joseph Harrison, and Dr. John Young for teaching me physics. I was very fortunate to have instructors who made difficult subjects interesting and enjoyable, and whose teaching challenged and motivated me. Special thanks to all my students who encouraged me to become a better teacher in so many ways.

I also would like to express my gratitude to Dr. Cheng Wang for his helpful discussion with me, Mr. Joseph Tombrello for his help on computer work, and Mr. David Gore for his help in the darkroom.

My appreciation also goes to Ms. Donna Hamer, Ms. Donna Andrews, Mr. Jerry Sewell, and Mr. Bill Little for their support for this research and throughout four years' study in the Department of Physics of UAB. Their help made study here pleasant.

Finally, I want to say special thanks to my husband, who supported and encouraged me to pursue my career 25 hundred miles away. Thank you, Hong; I could not have done it without you.

v

TABLE OF CONTENTS

TABLE OF CONTENTS (Continued)

CHAPTER   Page

LIST OF TABLES

LIST OF FIGURES

x

LIST OF FIGURES (Continued)

LIST OF FIGURES (Continued)

CHAPTER 1

INTRODUCTION

For many laser applications,[1-18] it is desirable for a light source to have a uniform energy profile. One of these applications is a laser projection system.[19-27] Such a projector can be used for writing mesh patterns on films and photosensitive substrates to produce filters and lens elements. If a non uniform laser beam is utilized, such as a Gaussian beam profile, the mesh pattern will have maximum energy density at the center and will trail off at the edge. Therefore, a uniform energy distribution is highly desirable. A prototype (proof-of-concept) of the laser beam reshaping system has been designed, assembled, and tested. The testing results have demonstrated that a two-plano-aspherical lens reshaper is an efficient and simple system. This reshaper is then integrated into a prototype of a holographic projection system. With the reshaping system, the projector produces four coherent, uniformly irradiance beams to generate the desired interference patterns.

Based on the performance of the prototype of the laser beam reshaper and the holographic projector, a UV laser reshaping system has been designed. It will be used in a UV projector of a production model which will produce optical arrays, filters, and other micro-optical elements. This UV projector has a much higher laser power and a much larger beam diameter than the prototype.

Many theories and technologies for reshaping a laser beam irradiance profile have been proposed and developed in recent years. [1-15] These theories include refractive lens systems,[4-5] reflective mirror systems,[6-8] holographic techniques,[9-11] beam

1

integrator,[12] Cylindrical Fly's Eye Lens(CFEL),[13] diffractive optics,[14] and gradient-index lens system.[15] Three commonly used reshapers are discussed below:

• Refractive lens systems

Beam reshapers of refractive lens systems use the surface shapes and the index of the lenses to reshape the beam profile. Some systems include two aspherical lenses;[4] others include four spherical lenses.[5] Rhodes and Shealy[4] reported in 1980 a refractive optical system for irradiance redistribution of collimated radiation, as shown in FIG 1.1. This system consists of two plano-aspherical lenses and can be designed to convert an arbitrary radially symmetric beam profile into a uniform beam profile with high energy efficiency, such as a Gaussian beam can be converted into a uniform beam without truncating the incoming beam energy.
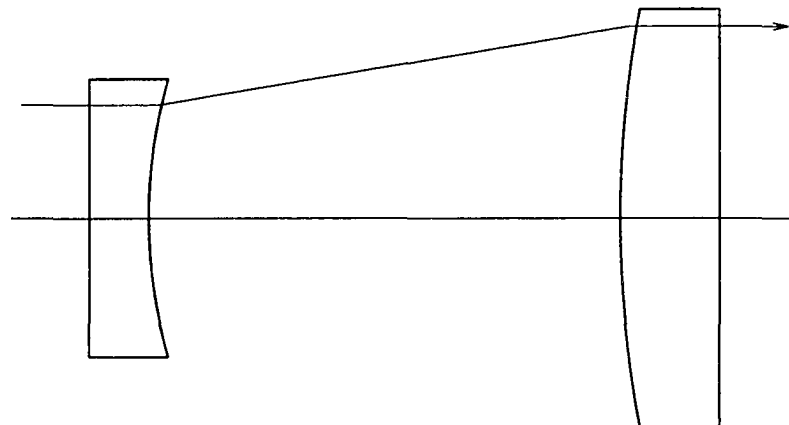
FIG. 1.1. Lens system proposed by Rhodes and Shealy.

Another reshaping refractive lens system proposed by D. Shafer[5] includes four spherical lenses as shown in FIG 1.2. This design avoids aspherical surfaces. However, it is harder to design and has at least eight spherical surfaces to be made. In addition, it has low energy efficiency which can only convert 63.2% (using the diameter at which the energy density is $1/e$ of the central value) of the Gaussian energy distribution into the outgoing beam.
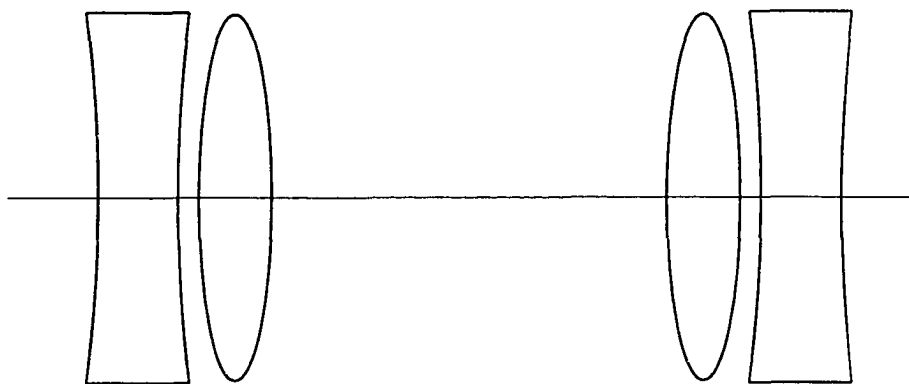
FIG. 1.2. Spherical lens system proposed by Shafer.

● Reflective mirror systems

For high power laser beam reshaping, lenses are replaced by mirrors. One of these systems proposed by J. Ogland[6] consists of two concentric mirrors (see FIG. 1.3). This system can reshape a high power laser beam, but it obviously wastes a lot of energy as a result of the central obscuration.
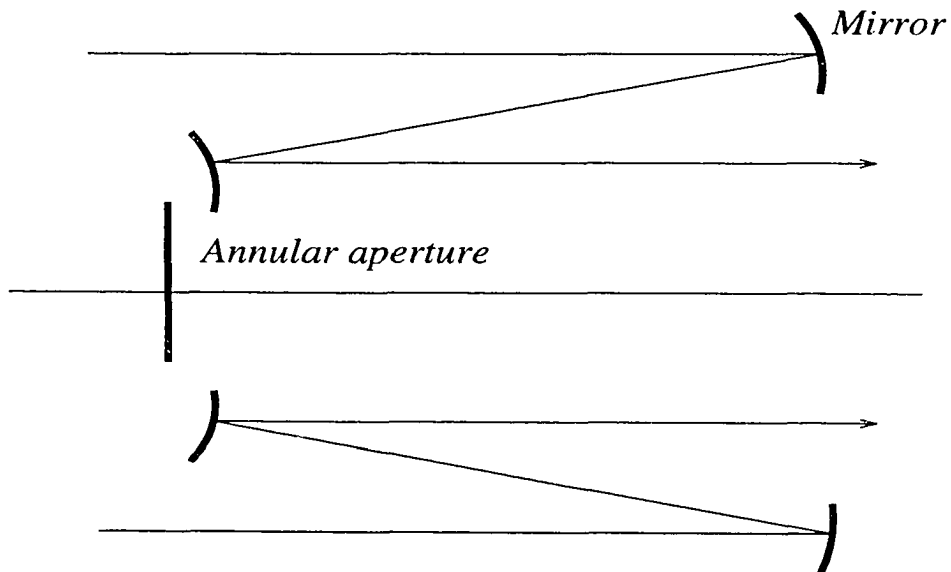
FIG. 1.3. Mirror system proposed by Ogland.

A reflective system proposed by P. Malyak[8] consists of two decentered mirrors (see FIG. 1.4). This system solves the problem of lost energy due to a central obscuration; however, it is difficult to manufacture due to the asymmetry of the mirrors.
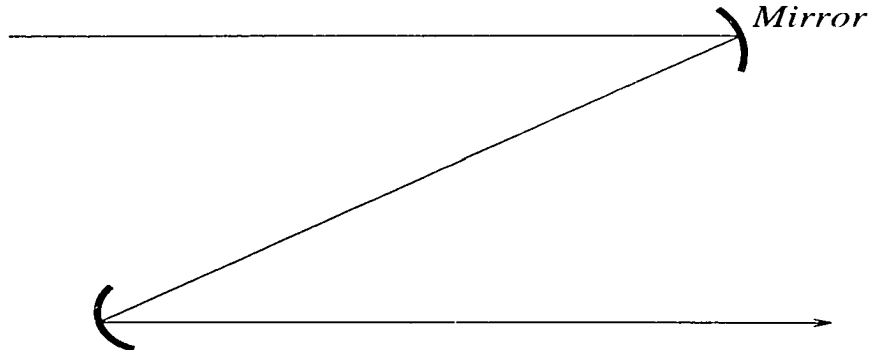
Mirror

FIG. 1.4. Mirror system proposed by Malyak.

• Holographic optical element system

The technique used by the holographic method is to design the holographic optical elements (HOE) so that the energy density profile is redistributed. In FIG. 1.5, HOE #1 is designed to produce a uniform intensity at the surface of the second element; then, HOE #2 acts as a phase corrector to produce a uniform output phase. This system can be made very compact. However, it has a low irradiance transformation efficiency due to the diffraction losses.

HOE # 1

HOE # 2
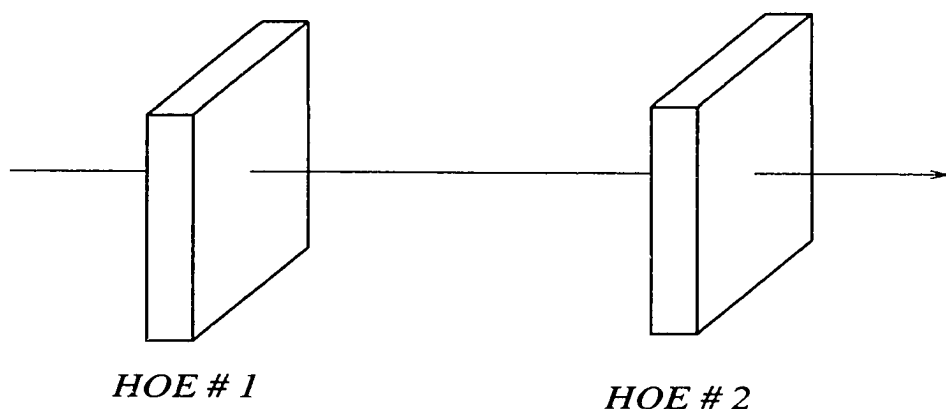
FIG. 1.5. Holographic optical element system.

Compared to these reshapers, the two-plano-aspherical lens system, which can be designed to convert an arbitrary radially symmetric beam profile into a uniform profile, is a simple system with high efficiency. The original disadvantage of this system was the difficulty in fabricating aspherical surfaces. With the development of the technology of manufacturing aspherical surfaces, it is possible today to make many shapes of aspherical lenses using single point diamond lathe cutting fixtures. Therefore, the two-aspherical-lens system has been chosen to reshape the laser beam profile for the holographic projector.

The two-plano-aspherical lens reshaper is shown in FIG. 1.6. It converts a collimated incoming beam profile, $\sigma\,(r)$, which is incident upon the primary lens at a radius r from the optical axis, into an output beam, $u\,(R)$, that leaves the optical system as a collimated beam at a radius R. In this study, $\sigma\,(r)$ is a Gaussian distribution, and $u\,(R)$ is assumed to be a constant, that is, a uniform profile. The aspherical surface of the primary lens deviates the plane wave, Gaussian input beam so that the intensity is uniform at the second lens. The second aspherical surface has no effect on the energy distribution but deviates the rays so that the outgoing wavefront is a plane wave like the input wavefront, which means that the outgoing wavefront has the same structure as the incoming beam.
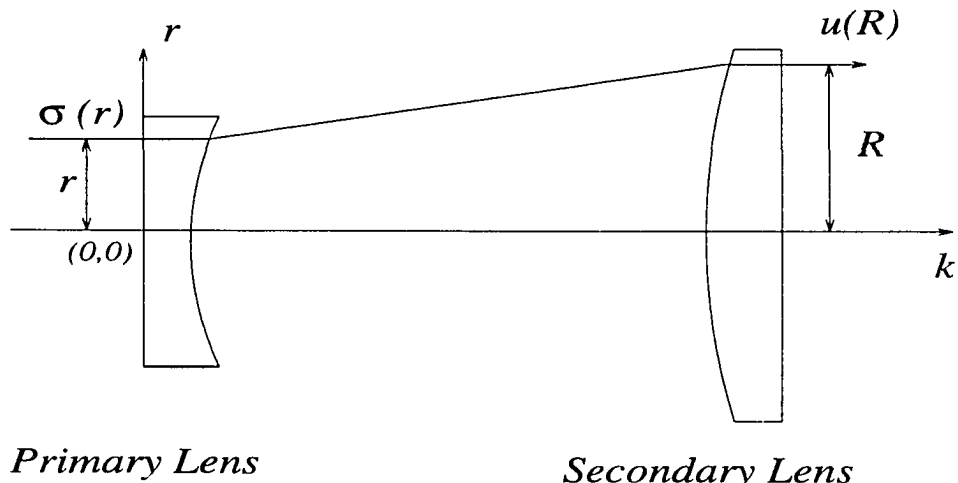
FIG. 1.6. The two-plano-aspherical lens system.

This reshaper has been integrated into a prototype of a holographic projection system shown in FIG. 1.7. This projector consists of a laser, an expansion system, a beam profile reshaper, a binary optical element (holographic differential grating), a prism system, and a detector which may be film or photosensitive substrate. The expansion system is used to enlarge the laser beam while the higher order noise is eliminated by a spatial filter inside the expander. After the laser beam has been reshaped from a Gaussian into a uniform profile, a binary optical element is used as a beam splitter. It divides the amplitude of the laser into four sets of spectral orders in four symmetric and diverging directions. The diverging beams have the same diameter and shape as the input beam. Eight prism wedges are used after the diffraction grating to recombine the beams. The recombined uniform and coherent beams then interfere to produce grid pattern at a detector (film or photosensitive substrate).

The holographic projector system has many applications. It can be used for the production of directional light filters, [23] which provides a whole new method of focusing light allowing magnification or demagnification while also removing aberrations and scattered light. It also can be used in producing tapered array microchannel plates (MCPs) which may be used in new and interesting designs of many types of CCDs.

The conventional methods[24-27] of holographic projection systems used in the past are based on dividing the laser into multiple beams. Two methods are commonly used: division of wavefront (DOW) and division of amplitude (DOA). Both methods utilize spatial filters to truncate the beam profile to achieve a uniform profile. These two methods are shown in FIGs. 1.8 and 1.9.

Expansion system

Laser

Spatial filter

Beam reshaper

Prisms

Detector

Binary optics
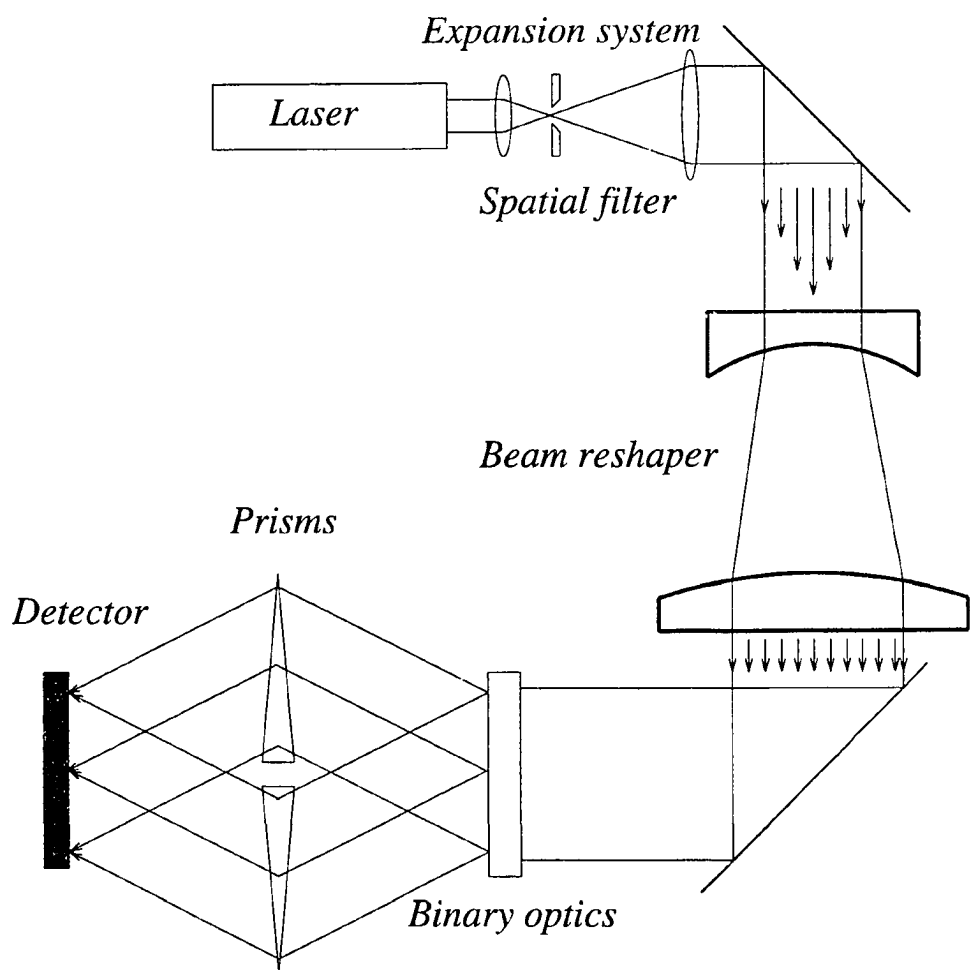
FIG. 1.7. The prototype of the holographic projector.

In FIG. 1.8, the three beam DOW setup uses three mirrors: M_1, M_2, and M_3. They are arranged equilaterally to intercept an expanded laser beam. The mirrors reflect the beams which are recombined at a point off axis of the incoming beam. The disadvantage of this system is the reduction of energy in each beam because the mirrors intercept only a proportion of the beam. In addition, a spatial filter is used to obtain a uniform profile, which has truncated part of the energy. Otherwise, the interference pattern will have maximum energy density at the center and will trail off at the edge. This system is also very difficult to align.
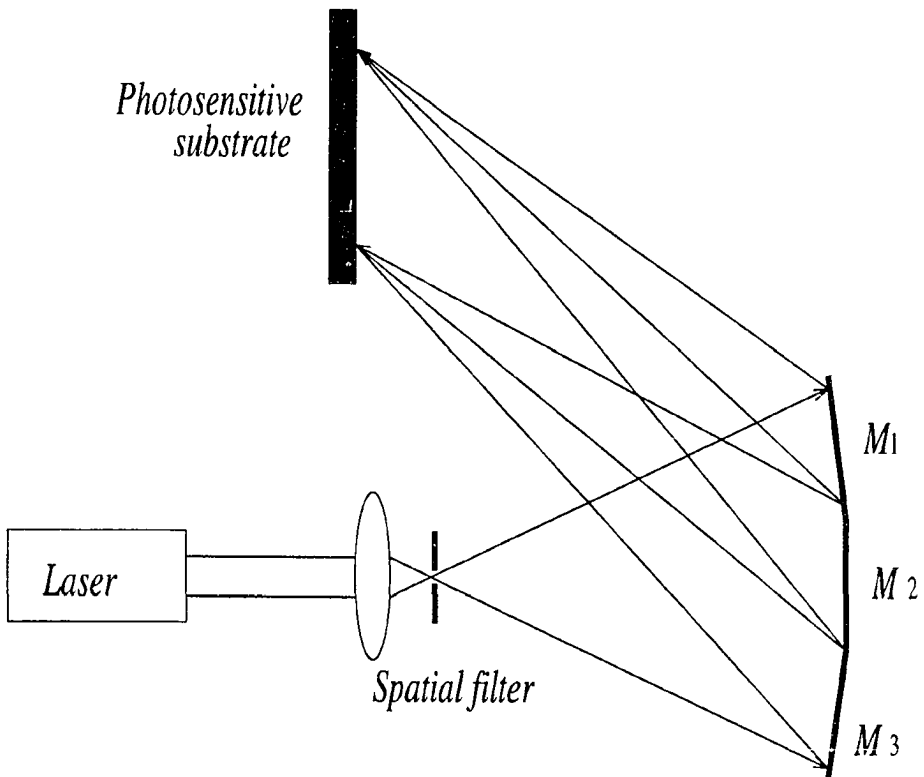
FIG. 1.8. Division of wavefront.

Another method is the DOA shown in FIG. 1.9. The multiple beams are obtained by the use of beam splitters. Then a spatial filter is used to obtain a uniform beam profile. Therefore, this system also loses part of the energy due to the desire for having a uniform laser beam profile. Similar to the DOW setup, the DOA method is also a rather complicated system to align.
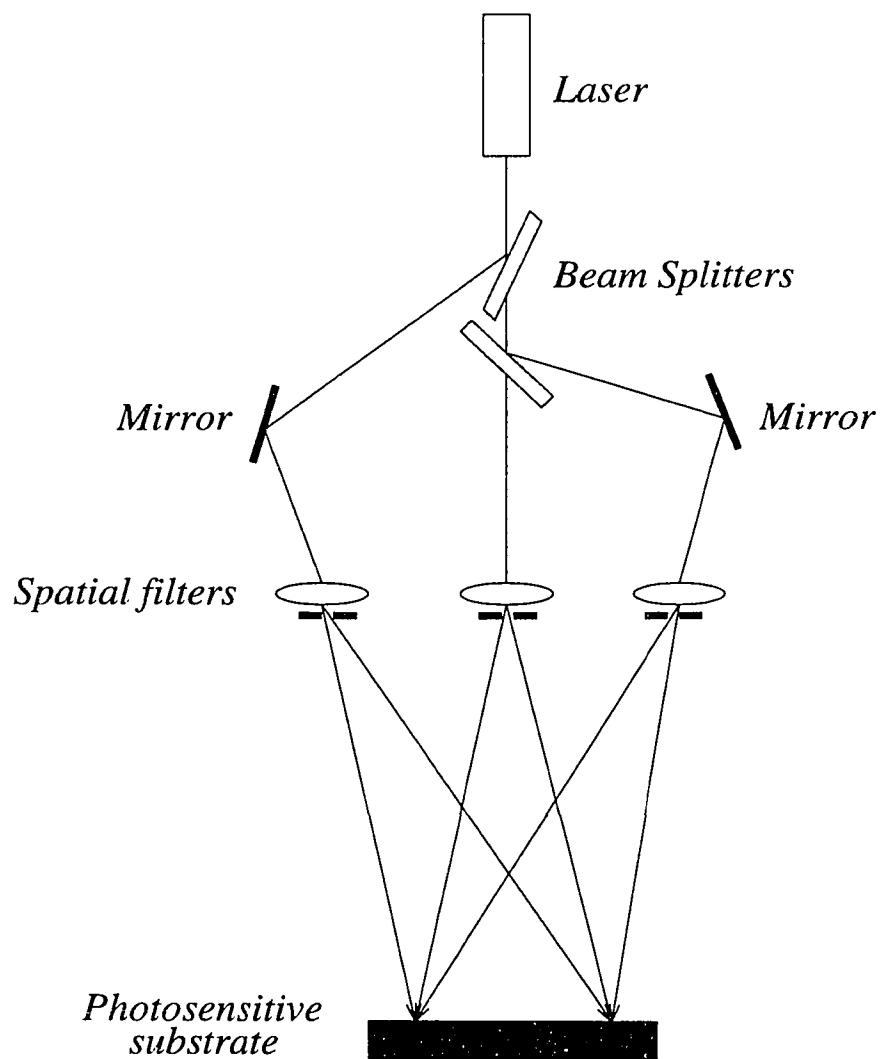
FIG. 1.9. Division of amplitude.

Compared to these holographic projectors, the projection system in this study, which is shown in FIG. 1.7, provides maximum energy efficiency since it utilizes a laser beam reshaping system to produce a uniform intensity profile instead of truncating the energy; it is also a very compact and simple system since it utilizes a diffractive grating to divide the beam without using traditional beam splitters and mirrors. These two distinctive factors of this projector make it possible for massive production of monolithic microchannel optical arrays because the elements can be produced over a large surface with a uniform grid pattern.

In the next chapter, the optical design and analysis of the reshaping system are first given. This design is based on two conditions: conservation of energy and constant optical path length. The flux-flow equation[28] as well as a conventional optical software, such as GENII-PLUS,[29] was used to analyze the performance of the reshaping system. Calculations have been done in section 2.1.1.4 to predict that one reshaping system can be used to reshape multiple wavelengths by simply varying the distance between the two aspherical lenses. Then a prototype of the holographic projection system, which uses the beam reshaper, is presented. The grating equation of a refractive phase grating used in this projector is derived in section 2.1.2. Since testing results of the prototype of the projection system have proven the design theories of both the reshaper and the projector, a UV beam profile reshaper of a laser projection system of a production model was designed. This design is similar to that of the prototype; however, the UV projector has a much higher laser power and greater beam size than the prototype due to the requirements of its applications. The binary optics is also different from the prototype since it is designed to produce a diverging lattice of hexagonal intensity maxima extending through the photosensitive substrate so that the substrate will contain a honeycomb-like grid after the standing wave image is recorded and fixed. Such a substrate can be used as directional light filters and micro-optical arrays.

In Chapter 3, testing results are presented. Experimental results of the reshaping system are given in section 3.1. These experiments include qualitatively testing the reshaper by a Helium Cadmium laser using a camera-film system and quantitatively testing using a camera-computer system which is supported by an imaging processing software. After the reshaping system was tested, a HeNe laser also was tested to provide evidence to support the prediction that one reshaper can be used to reshape multiple wavelengths. Then, acceptable tolerances of reshaping system also were studied by tilting and decentering these two aspherical lenses. In the second part of Chapter 3, the experimental results of the prototype of the holographic projection system are discussed. Testing results of this projector with and without the beam profile reshaping system are presented to demonstrate that the reshaping system has enhanced greatly the performance of the projection system. Summaries and conclusions of this study are given in Chapter 4.

The design, analysis, and testing results of the reshaping system demonstrate that a two-plano-aspherical lens system can efficiently convert an arbitrary radially symmetric beam profile into a uniform beam profile. In this study, a Gaussian beam was converted into a uniform beam. This reshaper was then integrated into a holographic projection system so that the interference grid patterns of this projector had a uniform energy distribution over the entire surface. The enhanced experimental results of the holographic laser projection system have shown the importance of the reshaper. With the reshaping system, the size of the grid has been increased greatly without degradation in the quality of the interference pattern, and the energy efficiency also has been increased significantly.

CHAPTER 2

THEORY

The holographic projection system produces multiple uniform and coherent beams to obtain desired interference patterns on photosensitive substrates or films. The uniform and coherent beams are results of utilization of a beam profile reshaping system and a binary optics which divides the wavefront of the beam into multiple beams. Such a system can be used in producing directional light filters, tapered arrays microchannel plates (MCPs), and monolithic optical arrays. This system is shown in FIG. 2.1.

In this chapter, the design theory and analysis of the projection system are presented. In section 2.1, the design and analysis of the prototype projector are given. It includes the design theory and analysis of the reshaping system of the projector, calculations which predict that one laser beam reshaper is capable of reshaping different wavelengths of light by simply varying the lens spacing of the two-plano-aspherical lenses, and the derivation of the grating equation of the diffraction grating which is used to generate four diverging, coherent spectral order beams. A UV laser projection system of a production model is presented in section 2.2. This system is a revised and improved system of the prototype, described in section 2.1. The production system will have greater laser power and a larger beam size than the prototype, and it will produce a more complicated interference pattern due to the design of the diffraction grating. The detector of the UV system will be a curved surface instead of a plane surface like the prototype. Section 2.3 summarizes the design theory of this projection system.

12
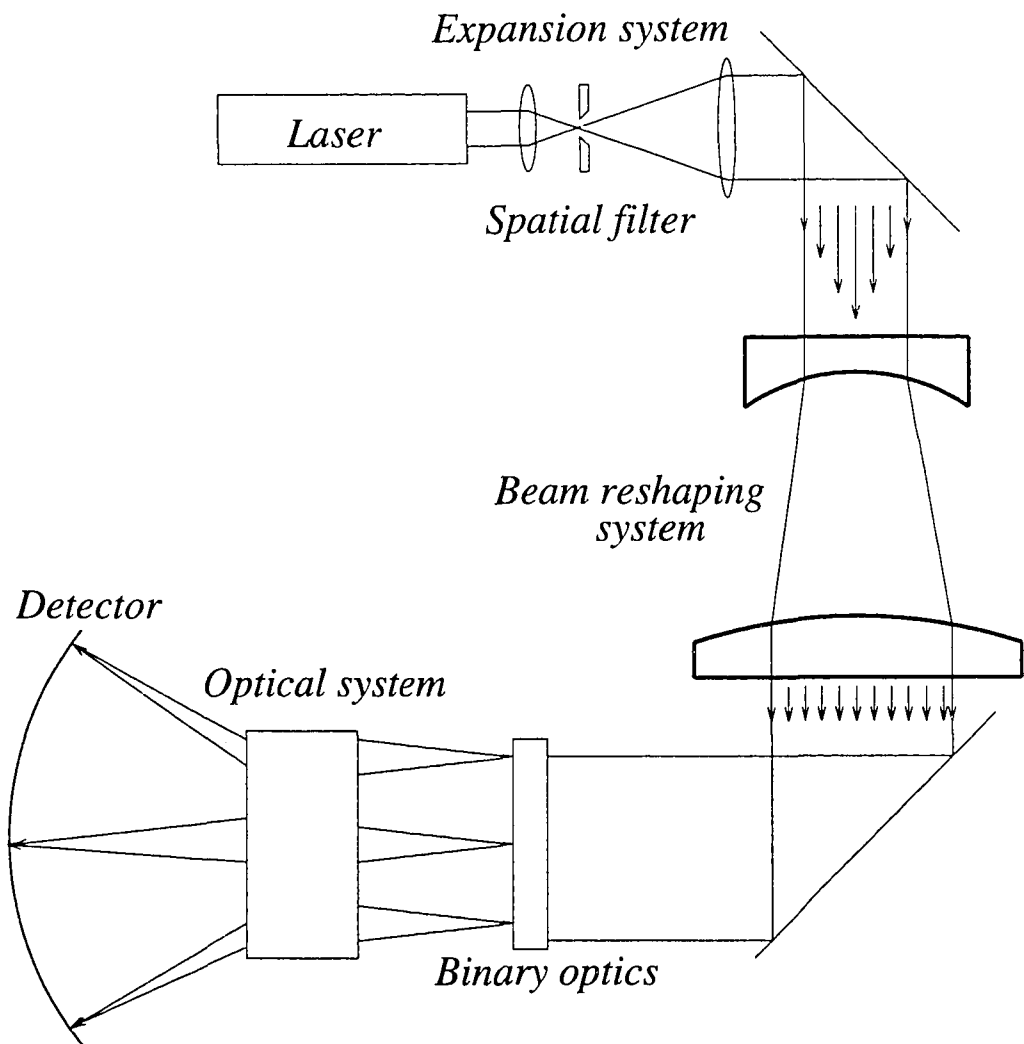
FIG. 2.1. The holographic projection system.

2.1. The prototype of the holographic projection system

A prototype of the holographic projector has been designed, fabricated, assembled, and tested. The key factors of this prototype are the reshaping system, which is a two-plano-aspherical lens system, and the binary optics, which is a two-dimensional, two-level diffraction grating. The design theory and analysis of the

reshaping system are represented in section 2.1.1, and the design of the holographic diffraction grating is discussed in section 2.1.2. This prototype of the holographic projection system is shown in FIG. 1.7.

2.1.1. The reshaper of the prototype

A beam profile reshaper, shown in FIG. 2.2, was used in this holographic projector to convert a collimated incoming beam with an energy per unit area $\sigma(r)$, which is incident upon the primary lens at a radius r from the optical axis, to an output beam that leaves the optical system as a collimated beam at a radius R with an energy per unit area $u(R)$ = constant. The aspherical surface of the primary lens deviates the plane wave, Gaussian input beam so that the intensity is uniform at the second lens. The second aspherical surface has no effect on the energy distribution but deviates the rays so that the outgoing wavefront is a plane wave as is the input wavefront, which means that the outgoing wavefront is retained from the incoming beam.

Primary Lens   *Secondary Lens*
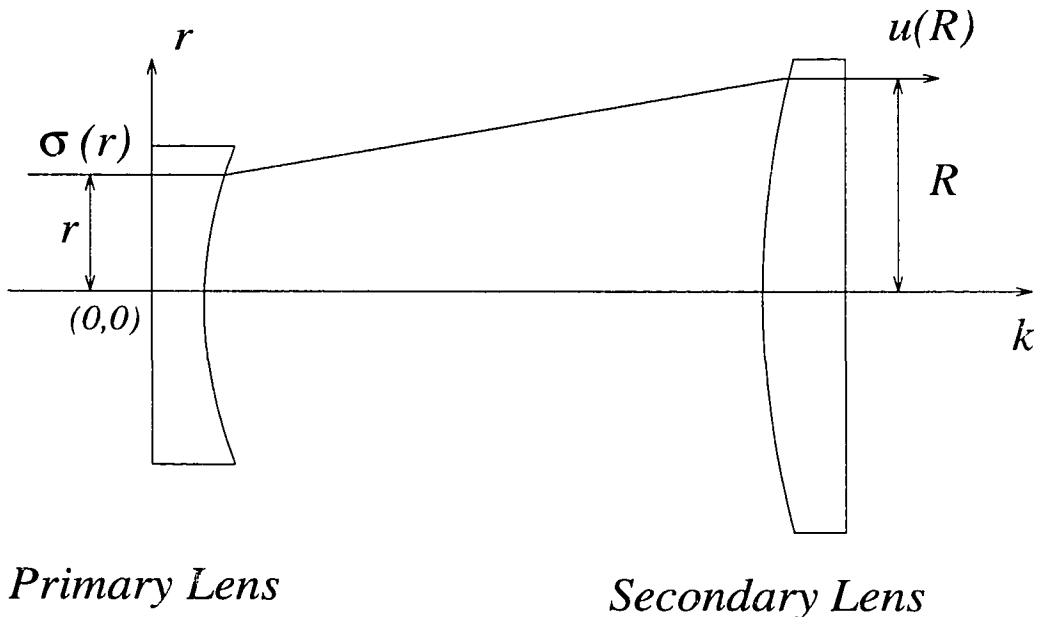
FIG. 2.2. Geometrical configuration for reshaping lens system.

2.1.1.1. Optical design. The design of the reshaping lens system was based on two principles: conservation of energy and constant optical path length condition.

2.1.1.1.1. Conservation of energy. The energy of the incoming beam should be totally transmitted to the outgoing beam, assuming transmission coefficient is η. This can be expressed by the following equation:

$$\int_0^{2\pi}\int_0^r \sigma(r)\,rdrd\theta = \int_0^{2\pi R}\int_0^{} u(R)\,RdRd\theta.$$

(2.1)

Since u(R) is constant, R can be solved from Eq. 2. 1 into Eq. 2. 2:

$$R = \sqrt{\frac{2}{u}\int_0^r \sigma(r)\,rdr},$$

(2.2)

where

$$u = \frac{2\eta}{R_0^2}\int_0^{r_0}\int_0^{} \sigma(r)\,rdr.$$

(2.3)

In Eq. 2.3, r_0 is the radius of the working aperture of the primary, and R_0 is the corresponding point on the secondary.

In this study, the incoming beam was a Gaussian mode (TEM_{00}), and the outgoing beam was uniformly distributed. For this fundamental mode, $\sigma(r) = \exp(-r^2/2\alpha^2)$ was chosen. This means that the central intensity is normalized to unity, $\sigma(0) = 1$. To specify the propagation characteristics of a laser beam, one has to define its diameter in some way. The commonly adopted definition[30] is the diameter where the transverse field amplitude has fallen to a fraction 1/e of its peak axial value. This is often called the waist of the beam. At this same diameter, the corresponding beam intensity will have

fallen to $1/e^2$ of its peak or axial value which includes 86.5% of the total energy of a Gaussian beam. This $1/e^2$ definition of a laser beam diameter has been used in the design and fabrication of a prototype laser reshaping optical system. If r_0 is used as the waist of the beam, then $\sigma(r_0) = \sigma(0)/e^2$. This leads to $r_0 = 2\alpha$. Therefore,

$$\sigma(r) = \exp(-2(r/r_0)^2). \tag{2.4}$$

Using Snell's law to calculate the direction of the refracted ray at surface s, a vector equation for **B** (FIG. 2.3) can be written as

$$\mathbf{B} = \gamma \mathbf{A} + \Omega \mathbf{n}, \tag{2.5}$$

where

$\gamma = n_1/n_0.$

$\mathbf{A} = \hat{k},$

$\Omega = -\gamma \mathbf{A} \cdot \mathbf{n} + \{1-\gamma^2[1-(\mathbf{A} \cdot \mathbf{n})^2]\}^{1/2},$

$$\Omega = \frac{-\gamma + [1 + (z')^2(1-\gamma^2)]^{1/2}}{[1 + (z')^2]^{1/2}},$$

$\mathbf{n} = [-z'\hat{r} + \hat{k}]/[1+z'^2]^{1/2},$

$z' = dz(r)/dr.$

n_1 is the index of refraction of the primary lens, and n_0 is that of the surrounding medium, which is air in this study. Therefore, $n_0 = 1$. $\mathbf{n}$ is the unit normal vector to the surface s.

In order to use energy conservation relationships between ray heights of the incoming and outgoing beams, one should use conventional ray tracing techniques to relate coordinates on the different lens surfaces. The transfer of the ray from surface s to surface S is given by the ray trace equations. As shown in FIG. 2.3, the equation of the

ray from (r, z) on surface s to (R, Z) on surface S is a straight line; therefore,

$$(R-r) B_z = (Z-z) B_r, \tag{2.6}$$

where B_r, B_z are the r, z components of **B**. Combining Eqs. 2.5 and 2.6 gives

$$z'^4[(1-\gamma^2)(Z-z)^2-\gamma^2(R-r)^2] + z'^3[2(R-r)(Z-z)] + z'^2\{[1-(\gamma^2)][(R-r)^2 + (Z-z)^2]\}$$

$$+ z'[2(R-r)(Z-z)] + (R-r)^2 = 0, \tag{2.7}$$

which can be factored to give

$$(1-\gamma^2)(Z-z)^2(1+z'^2)z'^2 + 2(R-r)(Z-z)(1+z'^2)z' + (R-r)^2(1-\gamma^2 z'^2)(1+z'^2) = 0. \tag{2.8}$$

Since z' is real, $(1 + z'^2)$ will not be zero. Therefore, Eq. 2.8 reduces to

$$[(1-\gamma^2)(Z-z)^2 - \gamma^2(R-r)^2]z'^2 + 2(R-r)(Z-z)z' + (R-r)^2 = 0. \tag{2.9}$$

This is a quadratic equation for z'. In Eqs. 2.6, 2.7, 2.8, and 2.9, R is given by Eq. 2.2.
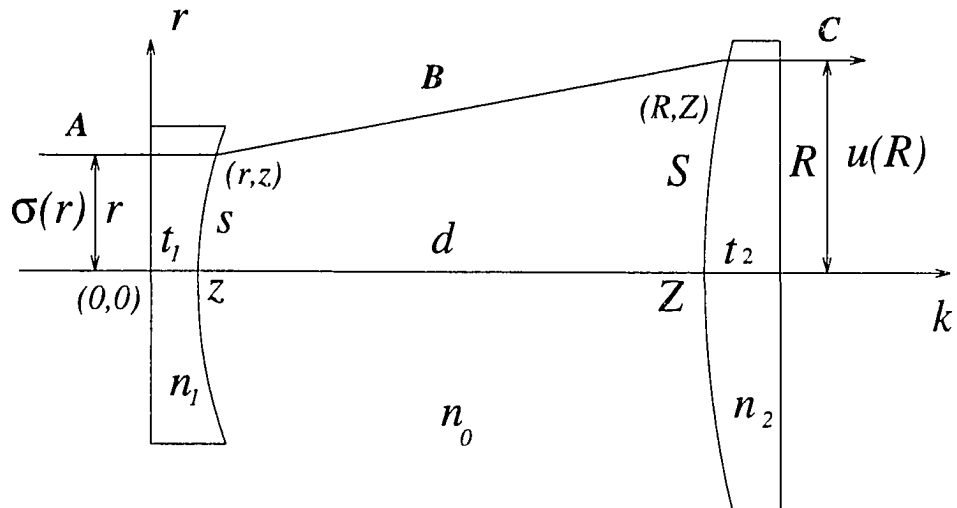
FIG. 2.3. Ray trace configuration of lens system.

Similarly, the refractive equation for the second lens can be written as

$$C = \gamma_2 B + \Omega_2 N, \qquad (2.10)$$

where

$C = \hat{k}$, (This collimates the outgoing beam.)

$\gamma_2 = n_0/n_2$,

$$\Omega_2 = \frac{-\gamma_2 \{\gamma z'^2 + [1 + z'^2 (1 - \gamma^2)]^{1/2} [1 + z'Z'] - \gamma z'Z'\}}{[1 + z'^2][1 + Z'^2]^{1/2}} + \frac{1}{[1 + Z'^2]^{1/2}},$$

$$N = \frac{-Z'\hat{r} + \hat{k}}{(1 + Z'^2)^{1/2}},$$

$Z' = dZ(R)/dR$.

n_2 is the index of refraction of the secondary lens. N is the unit normal vector to the surfaces S. Equation 2.10 can be solved to yield

$$Z' = \frac{\gamma_2 z' \{\gamma - [1 + z'^2 (1 - \gamma^2)]^{1/2}\}}{1 + z'^2 - \gamma_2 \gamma z'^2 - \gamma_2 [1 + z'^2 (1 - \gamma^2)]^{1/2}}. \qquad (2.11)$$

With the assumption of $n_1 = n_2 = n$ and $n_0 = 1$, Eq. 2.11 reduces to

$$Z' = z'. \qquad (2.12)$$

This indicates that for a given ray height r, the slopes of the interacting points at the two aspherical surfaces are equal if the same material is used for both lenses. This is obvious from Snell's law since the outgoing beam is required to be parallel to the incoming beam. The mathematical relationship between Z and z is determined by the constant optical path length condition, which is discussed in the next section.

2.1.1.1.2. Constant optical path length condition. In this optical system, the geometrical shape of the wavefront of the input Gaussian beam is retained. In other words, all rays passing through the optical system should have the same optical path length. Therefore, the exiting beam is a plane wave as is the incoming beam, and no wavefront aberration is introduced in the optical design. From FIG. 2.4, the optical path length (OPL) of the central ray equals to

$$OPL_1 = n_1 t_1 + n_0 d + n_2 t_2, \qquad (2.13)$$

and for an arbitrary ray

$$OPL_2 = n_1 z + n_0 [(R\text{-}r)^2 + (Z\text{-}z)^2]^{1/2} + n_2(d + t_1 + t_2 - Z). \qquad (2.14)$$
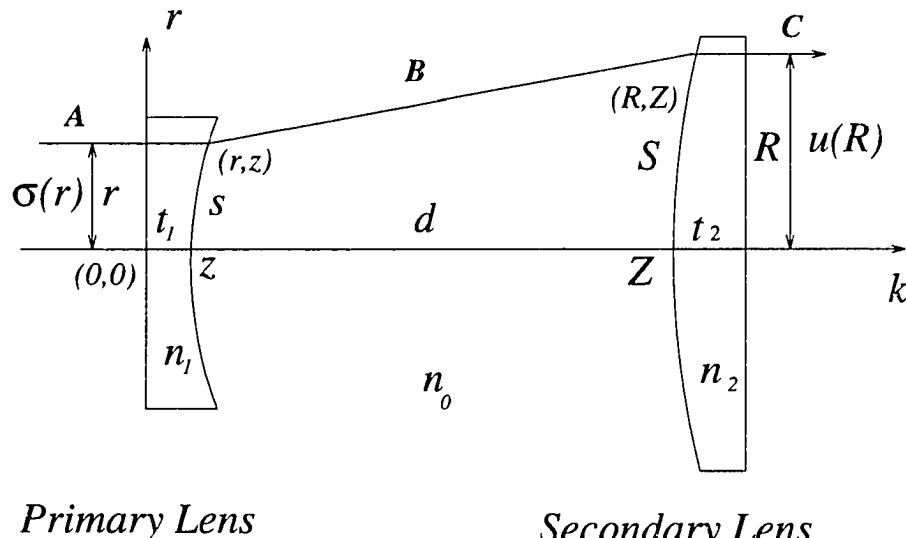
FIG. 2.4. Constant optical path length configuration.

The constant optical path length condition is satisfied for all rays passing through the system by requiring Eqs. 2.13 and 2.14 to be equal,

$$OPL_1 = OPL_2. \qquad (2.15)$$

Substituting Eqs. 2.13 and 2.14 into Eq. 2.15 gives

$$n_2 Z - n_1 z - n_0[(R - r)^2 + (Z - z)^2]^{1/2}$$

$$= n_2 (d + t_1 + t_2) - n_1 t_1 - n_0 d - n_2 t_2 \equiv K. \tag{2.16}$$

Since n_0, n_1, n_2, t_1, t_2, d are constants, K is also a constant. Rearranging terms and squaring, Z then can be solved from the above equation:

$$Z = \frac{(n_1 n_2 - n_0^2) z + n_2 K \pm n_0 [(K + n_1 z - n_2 z)^2 + (n_2^2 - n_0^2) (R - r)^2]^{1/2}}{n_2^2 - n_0^2}. \tag{2.17}$$

Equation 2.17 can be greatly simplified if $n_1 = n_2 = n$. This is a reasonable assumption for laser optics. Also, since the surrounding medium is air, $n_0 = 1$. This leads to

$$K = n (d + t_1 + t_2) - nt_1 - d - nt_2 = (n-1) d. \tag{2.18}$$

Therefore, Eq. 2.17 reduces to

$$Z = z + \frac{nK \pm [K^2 + (n^2 - 1) (R - r)^2]^{1/2}}{n^2 - 1}, \tag{2.19}$$

or

$$Z = z + \frac{n (n - 1) d \pm [(n - 1)^2 d^2 + (n^2 - 1) (R - r)^2]^{1/2}}{n^2 - 1}. \tag{2.20}$$

The physical solution for Z must satisfy the boundary conditions:

$$r = 0, z = 0;$$

$$R = 0, Z = d.$$

With these boundary conditions, Eq. 2.20 reduces to

$$Z = \frac{n (n - 1) d \pm [(n - 1)^2 d^2]^{1/2}}{n^2 - 1}$$

$$= d, \text{ when the positive root is chosen;}$$

$$= \frac{n - 1}{n + 1} d, \text{ when the negative root is chosen.}$$

Therefore, the positive root gives the physical solution:

$$Z = z + \frac{n(n-1)d + [(n-1)^2 d^2 + (n^2-1)(R-r)^2]^{1/2}}{n^2 - 1}. \qquad (2.21)$$

The surface shapes (r, z) and (R, Z) (FIG. 2.4) of the two aspherical surfaces can be obtained by solving the differential equations (Eqs. 2.2, 2.9, and 2.21).

2.1.1.2. Solution of differential equations for the optical design. The solution of the differential equations (Eqs 2.2, 2.9, and 2.21) will provide the shapes of the two aspherical surfaces which strictly satisfy the optical design conditions, where the transmission coefficient η is equal to 1. Different from the traditional optical design method, which optimizes the design parameters so that the optical aberrations are minimized, the method of solving differential equations gives an aberration-free solution.

From Eqs. 2.2, 2.9, and 2.21, R, z, z', and Z can be calculated. All of these are functions of r with given distance d and the index n. Solving these differential equations analytically appears to be very complicated, but it is straightforward to evaluate them numerically. Equation 2.9 gives

$$z'^2[(1-n^2)(Z-z)^2 - n^2(R-r)^2] + z'[2(R-r)(Z-z)] + (R-r)^2 = 0, \qquad (2.22)$$

which is a quadratic function of z' with coefficients consisting of lens index n, (R-r) and (Z-z). r, R, z, and Z (FIG 2.4) are variables. However, for a given r, Eq. 2.2 gives a corresponding value for R. After R is calculated, (Z-z) can be evaluated by Eq. 2.21. Therefore, it is straightforward to solve the quadratic function of z' numerically. Once z' is known, z can be obtained by the integral of z', and Z will be calculated by Eq. 2.21. Repeating these steps for a number of values of r provides an accurate description of surface shapes of the two aspherical lenses by numerical data (r, z) and (R, Z) (see Appendix A). Table 2.1 summarizes the design parameters of a prototype laser reshaping system. The precision of this description is determined by the accuracy of the evaluating method. In this study, the numerical error is less than 10^{-15}.[31]

Table 2.1. Parameters of a prototype laser system

Wavelength = 441.57 nm (HeCd laser)

Radius of the Working Aperture of the Primary = 8 mm

Radius of the Working Aperture of the Secondary = 12.5 mm

Distant Between the Lenses = 150 mm

Surrounding Medium Is Air, Index = 1.0

Index for the Two Lenses = 1.43916 (CaF_2)

Thickness of the Two Lenses = 10 mm

In Table 2.1, the thickness of the two lenses is given. Even though it is not in the design differential equations, it is an important factor to be considered since it relates to the energy absorption and manufacturing. For thicker lenses, there will be more energy lost as the result of the material absorption. On the other hand, very thin lens are harder to make and easier to break. So, these factors should be balanced. In the design of the prototype, the thickness of 10 mm has been chosen for both lenses.

2.1.1.3. Analysis of the optical performance for the design system. After solving the differential equations, it is desired to confirm that the two aspherical surfaces satisfy the design conditions, namely, conservation of energy and constant optical path length. Shealy and Burkhard[28] presented an analytical expression for the irradiance on a receiver surface due to rays that have passed through a multi-interface optical system. This technique is called the flux-flow equation, which is based on the geometry of the deflecting surfaces and the direction of the ray incident upon each surface. Using this theory, the flux-flow equation at the last surface of this system has been evaluated, and the results are represented in FIGs. 2.5 and 2.6.
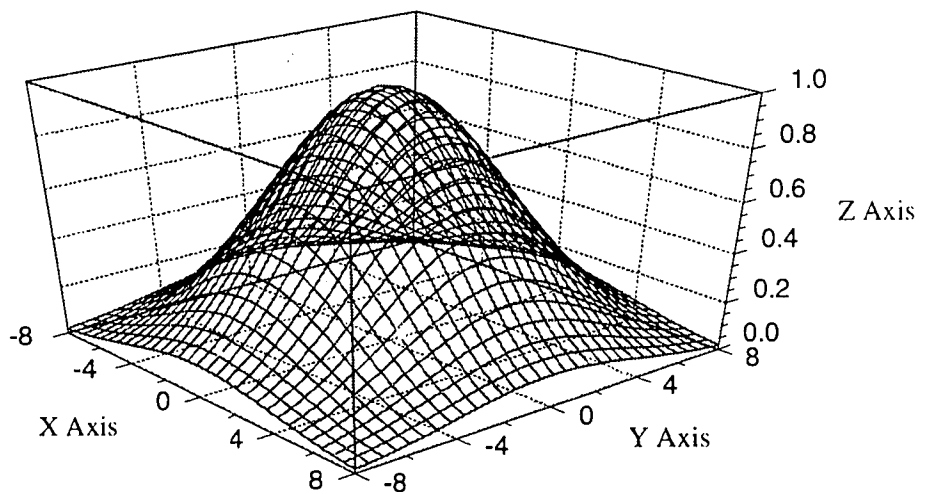
FIG. 2.5. Incoming energy profile of the reshaping system.
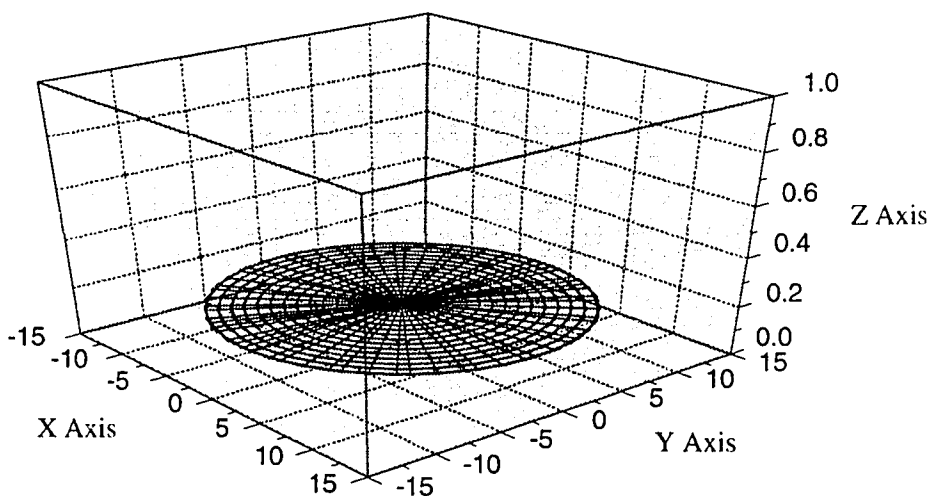
FIG. 2.6. Outgoing energy profile of the reshaping system.

Figure 2.5 shows that the incoming is a Gaussian beam, and FIG. 2.6 shows that the outgoing is a uniform profile. This is consistent with the design theory. If FIG. 2.6 is zoomed, the central cross section of the outgoing beam shows that it is not perfectly uniform, as shown in FIG. 2.7. The outgoing beam is not perfectly uniform because of the numerical errors in evaluating surface shapes; however, the maximum difference in the outgoing beam intensity was calculated to be less than 0.03%. This error is much less than that of the manufacturing; therefore, it is acceptable.
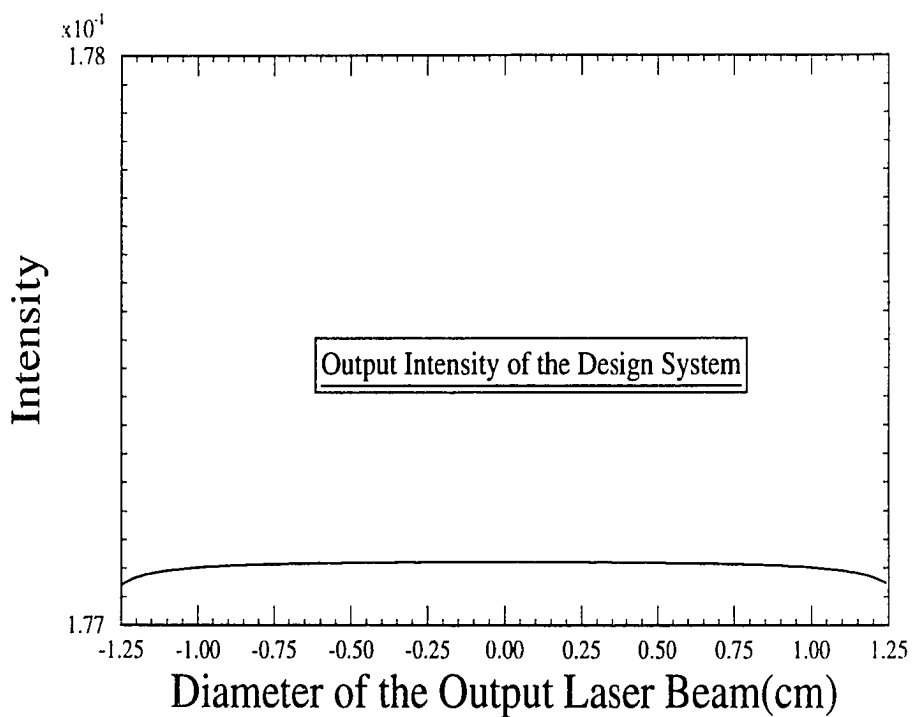
FIG. 2.7. Central cross-section of the output energy profile.

2.1.1.4. Application of multiple wavelengths to the reshaping system. Before solving the differential equations for a special case, the distance between the vertexes of the two aspherical surfaces and the material, n, of the lenses should be decided. Several factors must be considered when determining which criteria should be used and evaluating how different values for d and n will affect the system performance.

The distance between the lenses is not only important for optical design but is also a key parameter to consider during fabrication and testing. In the optical design, by varying the distance, the vertex curvatures and the asphericity of the surfaces will change. The larger the distance between the two lenses, the less will be the curvatures and asphericity of the lenses. This is important because large curvatures should be avoided since these surfaces are hard to make. However, if the lens spacing is too large, the whole system will be too long, and it will be inconvenient for users and harder to assemble and test. Considering these different aspects, the distance between the two lenses has been chosen arbitrarily to be about five times of the diameter of the lens substrate. For a specific example, if the diameters of the two lens substrates are 30 mm, then the lens spacing would be 150 mm.

The primary consideration for selecting the lens material is the transmission it exhibits within the region of intended use. This design is based on the application of the holographic projection system, which uses a Helium Cadmium laser with a wavelength of 441.57 nm. There are several materials which have very good transmission properties within this wavelength.[32] These material are Acrylic (PMMA) Plastic, Calcium Fluoride (CaF_2), Crown Glass (BK 7), LiF, Fused Quartz, and Fused Silica. Acrylic Plastic is too hard to polish. Fused Quartz, Fused Silica, and Crown Glass are difficult to machine with a single-point diamond lathe. LiF would be a poor choice because of the defects of the material. Considering these factors, CaF_2 has been chosen as the lens material. It transmits efficiently from 150 nm to 9000 nm (about 95%). It is easy to make and also is the least expensive material[32] option available for the wavelength of 441.57 nm.

The index of CaF_2 is a function[33] of wavelength being used:

$$n^2 = 1 + \sum_{i=1}^{3} \frac{A_i \lambda^2}{\lambda^2 - \lambda_i^2}, \tag{2.23}$$

where λ is measured in units of microns (μ);

$\lambda_1 = 0.050263605\mu$, $\lambda_2 = 0.1003909\mu$, $\lambda_3 = 34.649040\mu$;

$A_1 = 0.5675888$, $A_2 = 0.4710914$, $A_3 = 3.848723$.

Using Eq. 2.23, the refraction index of CaF_2 can be calculated, and it is 1.43916 for the wavelength of 441.57 nm.

Since the refractive index of the lenses is a function of wavelength, it will change when the reshaping system is used with lasers which have different wavelengths. Figure 2.8 shows an example of the wavelength being changed form λ to λ'. If this system is used to reshape a wavelength of 632.8 nm Helium Neon laser, the refraction index of CaF_2 will be 1.43289. Therefore, the rays will not strike at the same points of surface S as when wavelength of 441.57 nm light is used.
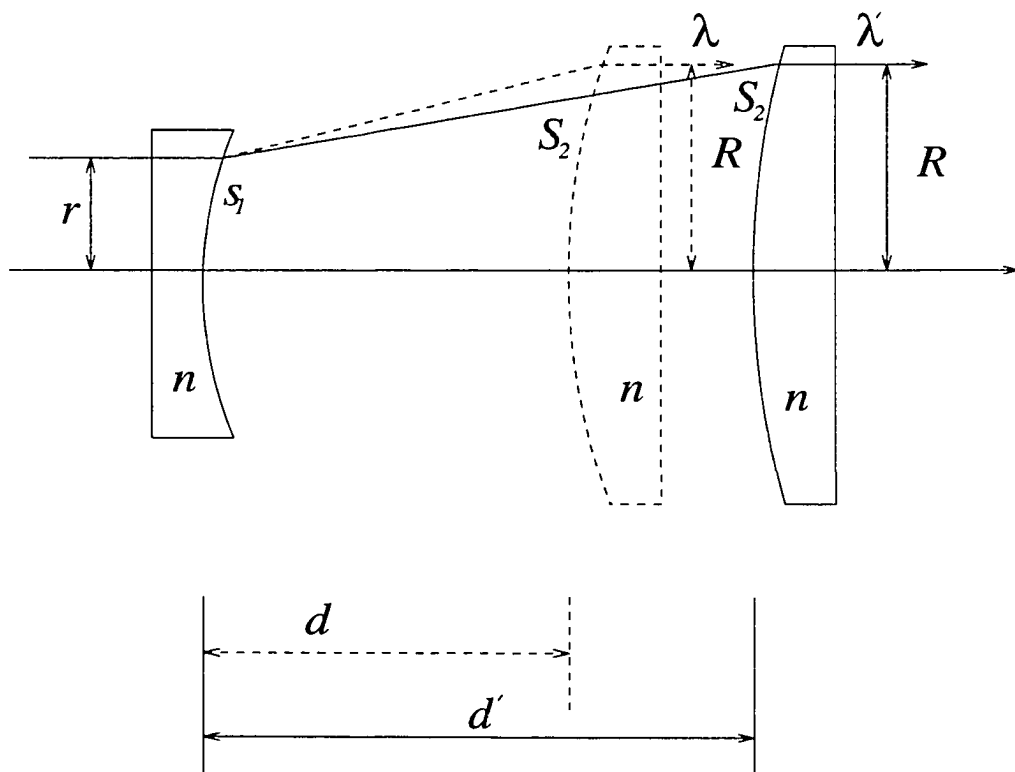
FIG. 2.8. The relationship between the wavelength and the lens spacing.

From Eq. 2.9, it is clear that the surface shape depends on the lens refractive index. Therefore, a system which is designed for a particular wavelength cannot be applied to reshape another laser beam uniformly. However, the effect on the reshaping performance due to the index changing can be reduced by varying the distance between the two lenses. For instance, it is possible to vary the distance between the lenses for a particular ray so that it is incident upon the design point of surface **S**. The new distance d can be calculated from Eq. 2.9. For a specific ray r, Eq. 2.2 determines R. So, r, R and z' are known. Therefore, Eq. 2.9 is a quadratic equation of (Z-z), which can be written as

$$(1-n^2)z'^2(Z-z)^2 + 2(R-r)z'(Z-z) + (R-r)^2(1-n^2z'^2)=0. \tag{2.24}$$

The solutions of (Z-z) are the following:

$$Z-z = \frac{(R-r)\,[1 \pm n\sqrt{1 + (1-n^2)z'^2}]}{(n^2-1)z'}. \tag{2.25}$$

The root using the negative sign gives negative values of (Z-z) for $z'>0$, which are not applicable to the physical situation. Therefore, the physical solution is

$$Z-z = \frac{(R-r)\,[1 + n\sqrt{1 + (1-n^2)z'^2}]}{(n^2-1)z'}. \tag{2.26}$$

Once (Z-z) is known, the corresponding value of d can be solved from Eq. 2.21, which can also be written as a quadratic equation of d:

$$(n^2-1)(n-1)^2 d^2 - 2n(n-1)(n^2-1)(Z-z)d + (n^2-1)^2(Z-z)^2 - (n^2-1)(R-r)^2 = 0. \tag{2.27}$$

The solution is

$$d = \frac{n(Z-z) \pm \sqrt{(Z-z)^2 + (R-r)^2}}{n-1},$$ (2.28)

where $n - 1 \neq 0$.

There are two roots for the distance d. Again, the physical solution must satisfy the initial conditions, which are when r = 0 and R = 0, (Z-z) = d. Therefore, the root with the negative sign is chosen:

$$d = \frac{n(Z-z) - \sqrt{(Z-z)^2 + (R-r)^2}}{n-1}.$$ (2.29)

The lens spacing d, given by Eq. 2.29, makes a particular ray remain parallel to the optical axis after leaving the system. However, every ray requires a different value of d to achieve the same characteristic. The question is by how much do different d values vary. If the difference is smaller than the assembling tolerance, then it would be possible for the same reshaping system to be used for other applications as long as the material of the lenses exhibits good transmission for those wavelengths. In this example, CaF_2 has very good transmission for both wavelengths of 441.57 nm and 632.8 nm.

Calculations have been done to show the changing of the lens spacing when a different wavelength is used. For instance, if a system with lens spacing of 150 mm is designed for a 441.57 nm Helium Cadmium laser, it is desired to change the lens spacing to approximate 152.2 mm when the system is used to reshape a 632.8 nm Helium Neon laser. This calculation is shown in FIG. 2.9. It is clear that for each ray, the lens spacing d is not the same. However, the maximum difference between the distances for all ray is less than 10 microns, which is smaller than alignment errors. This implies that the system designed for a Helium Cadmium laser should be able to reshape uniformly a Helium Neon laser by changing lens spacing.
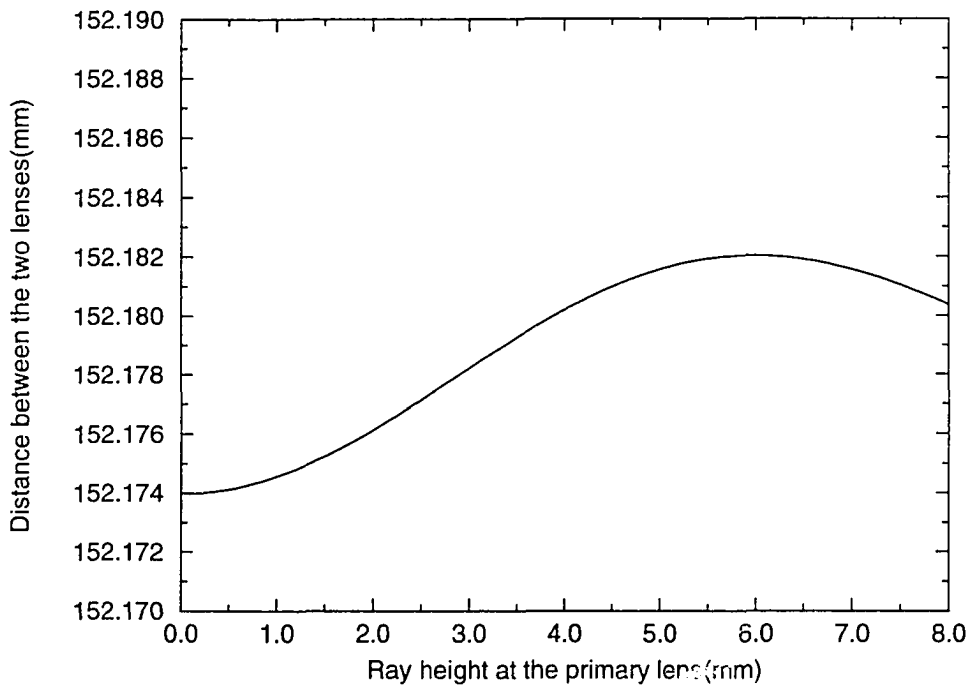
FIG. 2.9. Lens spacing for reshaping a HeNe laser.

2.1.1.5. Fitting process. After solving the differential equations (Eqs. 2.2, 2.9, and 2.21), the two aspherical surfaces of the lens system are represented by sets of numerical data [(r, z) and (R, Z)]. Although some aspherical surfaces can be fabricated directly from numerical data, it is more convenient to program a numerically controlled, single-point diamond lathe, if the aspherical surface can be expressed as an analytical function. For testing, it is convenient to use the optics surface equation[29] of a conic term plus rotationally symmetric aspherical deformation terms. Therefore, a non linear fitting method has been used to fit the surface data into the conventional optics surface equation.

2.1.1.5.1. The fitting method. There are several ways to fit the surface data. One of them is to use the cubic spline polynomial to fit the data. This approach can fit the data very accurately, but a given cubic spline polynomial fits the data over a small region of the surface. Therefore, it has not served the purpose of fitting the numerical data into an analytical formula for the entire surface. One can also use different linear fitting programs to fit different variables separately. This makes the fitting procedure rather complicated. In this study, a non linear least squares fitting program is used. This program calculates the non linear least squares to fit sampled data to a desired formula using the simplex method.[34] This method fits the surface data into the optical surface equation:

$$z = \frac{cr^2}{1 + \sqrt{1 - (1 + \kappa) c^2 r^2}} + \sum_{i=2}^{n} A_{2i} r^{2i}, \tag{2.30}$$

where c, κ, A_{2i} are the surface parameters that are determined by the fitting process.

Optical surfaces can be spheres, conics, and general aspheres. The equation above describes a general aspherical surface. The z is an even function of radius r. The curvature of the vertex (c), the conic constant (κ), and the coefficients of the polynomial deformation terms (A_{2i}) are the parameters to be determined. The first term represents the conic section, and the summation terms together with the conic section are used to represent general aspheres. If κ and A_{2i} are zero, which is a very special case, the surface will be a sphere with the radius equals to $1/c$. If κ is not zero, but A_{2i} is zero, this surface is a purely conic section such as ellipse ($\kappa > 0$, or $-1 < \kappa < 0$), parabola ($\kappa = -1$), and hyperbola ($\kappa < -1$). For a general asphere, κ is not zero, and a certain number of polynomial terms are needed. The number of polynomial terms which should be added to this formula depends on the shape of a surface. If a surface is close to a conic section, or a sphere, it will require fewer terms. If the shape of a surface is far away from a conic section, more polynomial terms will be needed for a better representation. Once the

shape of a surface (represented by a set of numerical data) is given, the curvature of the vertex is almost fixed. This is because the curvature is decided by the vertex data. However, κ and the A_{2i}s can have different solutions which are dependent on each other. In other words, there is not a unique solution for fitting a surface. If κ is changed, A_{2i} will change correspondingly in order to represent the same surface. Therefore, how to judge a fitting result becomes very important. From the point of view of the fitting process, as long as the analytical function represents the numerical data accurately, the fitting has done a good job. But from the point of view of manufacturing, it is desirable to use a small number of aspherical terms. For instance, a surface which is very close to a sphere can be represented both by a small conic constant plus a few polynomial terms, and a zero conic constant plus several more polynomial terms. If both represent the data equally well, it would be better to use the representation with fewer aspherical deformation terms for manufacturing. Therefore, for a specific system, it is desirable to identify simple surface representation which will reduce manufacturing difficulties while providing the same optical performance.

2.1.1.5.2. The fitting results. In the prototype of the reshaper, the laser beam is expanded from 16 mm to 25 mm in diameter while the beam profile is being reshaped. The lens substrate material is CaF_2. The fitting parameters of this system are given in Table 2.2.

The surface data have been fitted to many different expressions. More aspherical terms would give a better fit. However, manufacturers prefer fewer aspherical terms with a conic constant. The data in Table 2.2 with conic constant plus five aspherical terms represent a compromise between fitting accuracy, optical performance, and the ability to be manufactured.

Table 2.2. Fitting parameters of a prototype laser beam reshaper

Wavelength = 441.57 nm

Radius of the Working Aperture of the Primary = 8 mm

Radius of the Working Aperture of the Secondary = 12.5 mm

Distant Between the Lenses = 150 mm

Surrounding Medium Is Air, Index = 1.0

Surface Parameters

Lens Surface	Primary	Scondary
Diameters(mm)	30.0	30.0
Vertex Radii(mm)	47.86145	113.64905
Index	$1.43916(CaF_2)$	$1.43916(CaF_2)$
Thickness(mm)	10.0	10.0
Conic Constant	-1.11436	-1.48771
$A_4(mm^{-3})$	-7.15329×10^{-5}	-2.63246×10^{-6}
$A_6 (mm^{-5})$	3.37298×10^{-7}	9.40588×10^{-9}
$A_8(mm^{-7})$	-1.49168×10^{-9}	-2.3098×10^{-10}
$A_{10}(mm^{-9})$	5.98365×10^{-12}	1.58396×10^{-12}
$A_{12}(mm^{-11})$	-1.51665×10^{-14}	-4.84387×10^{-15}

2.1.1.6. Analysis of the optical performance. Since the aspherical surfaces have been fitted by an analytical formula, this system can be analyzed by both the flux-flow method as well as widely used optical software such as GENII-PLUS.[29] By the flux-flow equation, similar results have been obtained comparing with the numerical system in FIGs. 2.6 and 2.7. It is shown in FIG. 2.10. The optical path difference (OPD) of the outgoing wavefront was also evaluated with GENII-PLUS. The result of maximum OPD was 0.0017 wavelength, which suggested that the outgoing wavelength was almost

a plane wavefront. For the wavelength of 441.57 nm, the absolute OPD was about 0.75 nm. This error was due to the computational errors of the numerical methods; however, for such a small OPD, the wavefront of the incoming beam is almost retained.
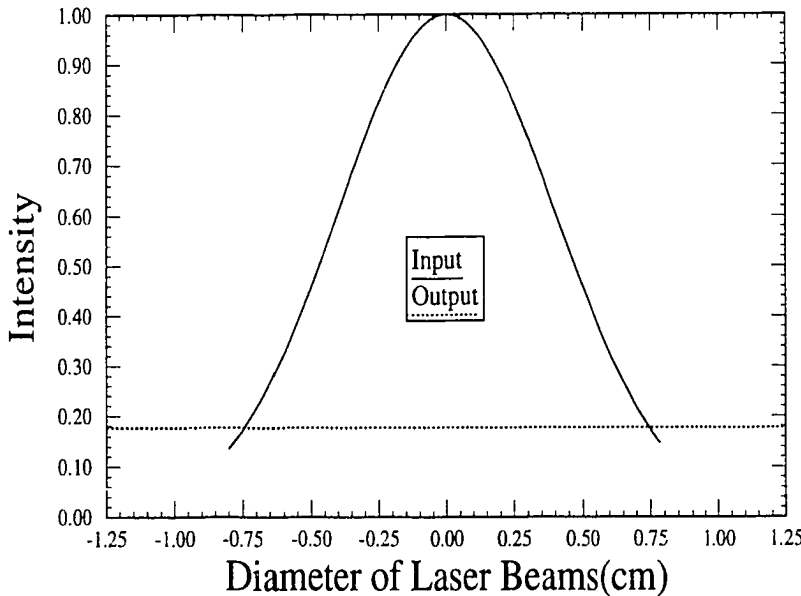
FIG. 2.10. Energy profile at the central cross-section of the fitting system.

2.1.1.7. Comparison between the designed and the fitted system. Figure 2.10 shows a combination of the two central cross sections of FIGs. 2.5 and 2.6. When expanding the scale of the fitted system, the outgoing beam is not perfectly uniform. The dot curve in FIG. 2.11 represents the outgoing profile of the fitted system. It is compared to that of the design system. It is clear that the outgoing beam of the fitted system oscillates at the edge. If more aspherical terms are added, it may reduce the oscillation. Since the manufacturer has difficulties handling more aspherical terms, the aspherical terms have been reduced to five plus a conic constant. However, the error of this fitting system is less than 0.2%. Nevertheless, the edge problem can be reduced by fitting a system in which the beam diameter is larger than the required beam size. If only the central part of the beam is used, the edge problem will be avoided.
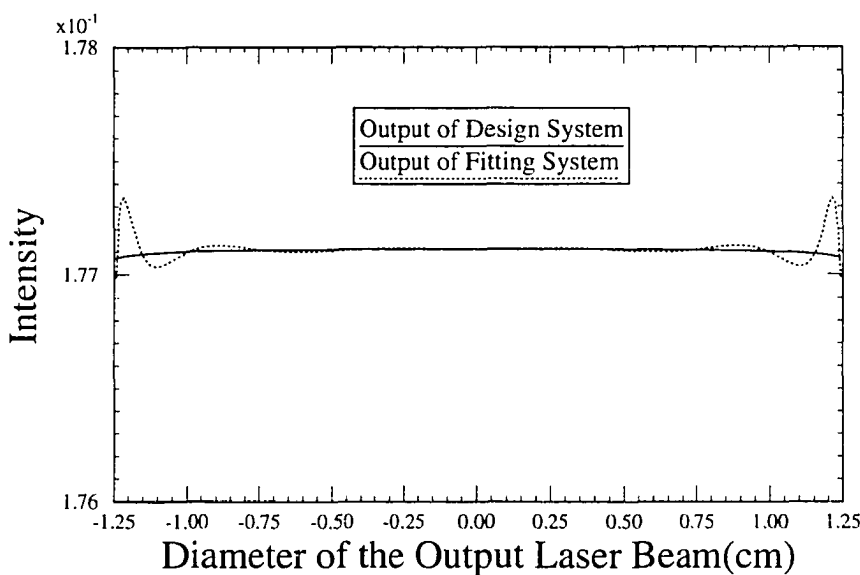
FIG. 2.11. Comparison between the design and fitting system.

2.1.2. The holographic diffraction grating

A diffraction grating may be defined as any arrangement of structures which imposes on an incident wavefront a periodic variation of amplitude or phase, or both. [35-40] A diffraction grating can be used to separate a wave motion into different spectral orders. Figure 2.12 illustrates a typical refractive diffraction grating. The grating constant is defined as the period of the grating, which determines the directions of the diffracted spectral orders. These diffracted directions of the spectral orders can be calculated by the grating equation[35]

$$d(\sin i \pm \sin \theta) = m\lambda, \qquad (2.31)$$

where i is the incident anlage, θ is the diffraction angle, integer m is the number of the diffraction order, and λ is the wavelength of the incident wave. The "+" sign will be used when the incident wavefront and diffracted wavefront are on the same side of the

normal line of the grating; the "-" sign will be used for the other case. The zero-diffracted order is in the direction which satisfies Snell's law.

Diffracted wavefront

Incident wavefront

θ

i

Grating constant d
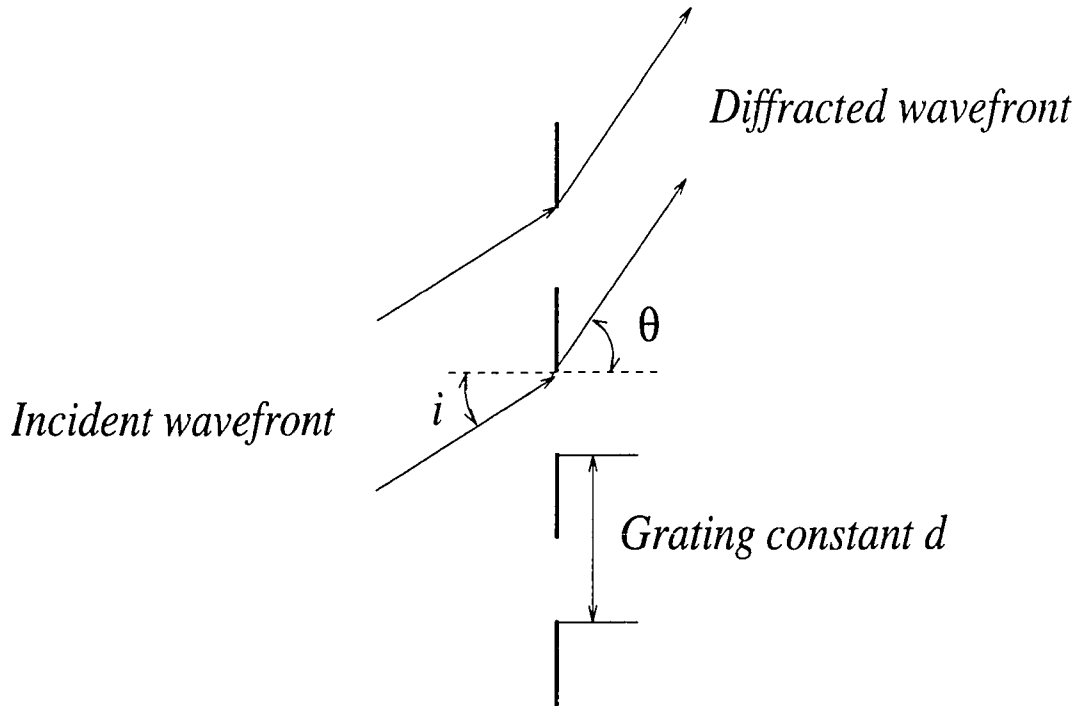
FIG. 2.12. Illustrating the theory of diffraction grating.

Some of the light is absorbed by the opaque strips in such a diffraction grating. To improve the energy efficiency, a strip of transparent material with an optical thickness (i.e., physical thickness times refractive index) is introduced to replace the opaque strip. Such a grating is known as "phase grating" or "phase generator." In FIG. 2.13, a one-dimensional, two-phase-level grating is presented. The phase difference between the two levels determines the etch depth h shown in FIG. 2.13.

The directions of the diffracted orders of such a phase generator no longer obey the grating Eq. 2.31. To illustrate the deriving procedures, FIG. 2.14 shows an enlarged drawing of one cell of such phase grating.
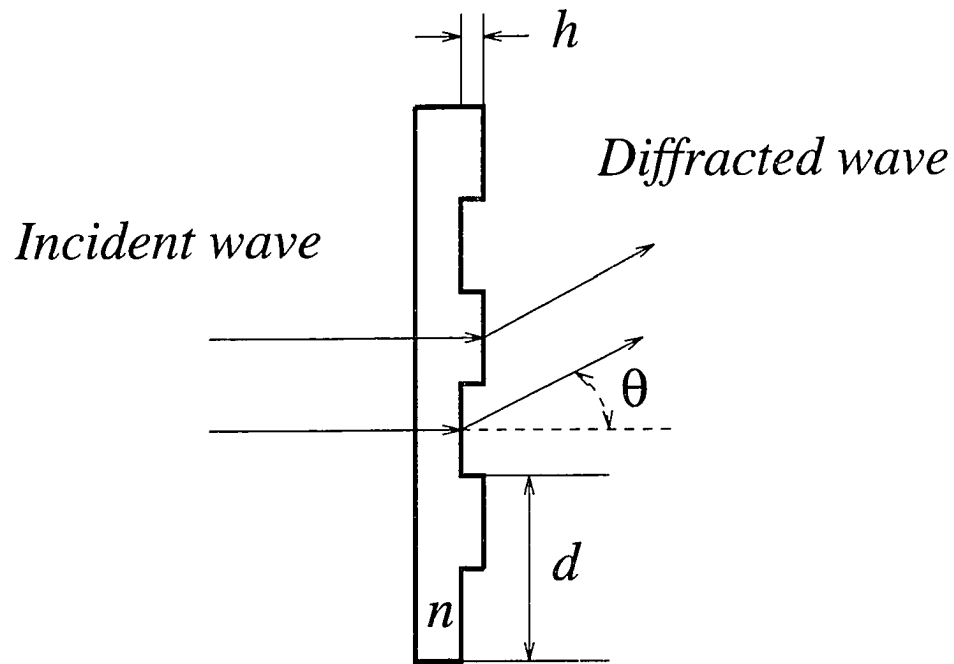
FIG. 2.13. The schematic drawing of a phase grating.
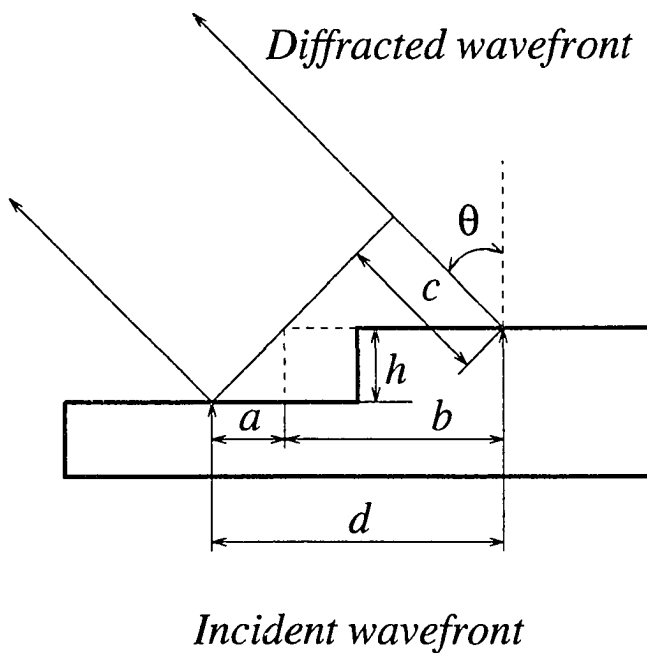
FIG. 2.14. The enlarged one cell of a phase grating.

In FIG. 2.14, assuming the diffracted angle is θ, the optical path difference between light arriving at the distant point of observation from corresponding point in two neighboring grooves is

$$\Delta = nh + c, \tag{2.32}$$

where h is the etch depth, n is the refractive index of the grating, and c can be obtained from the relationships among a, b, d, h, and θ. The derivation is shown in the following steps:

$$a = hctg\theta, \tag{2.33}$$

$$b = d - a = d - hctg\theta, \tag{2.34}$$

$$c = b\sin\theta = d\sin\theta - h\cos\theta. \tag{2.35}$$

Therefore, the optical path difference is obtained:

$$\Delta = nh + d\sin\theta - h\cos\theta = d\sin\theta + h(n - \cos\theta). \tag{2.36}$$

Thus, the grating equation for the phase generator can be written as

$$d\sin\theta + h(n - \cos\theta) = m\lambda, \tag{2.37}$$

where the integer m is the order of the interference, and λ is the wavelength of the incident wave.

If the direction of the diffracted wave is toward the unetched side, a similar derivation can be done, and the grating equation is

$$d\sin\theta - h(n - \cos\theta) = m\lambda. \tag{2.38}$$

Combined Eqs. 2.37 and 2.38, the grating equation of such a phase generator can be summarized as

$$d\sin\theta \pm h\,(n - \cos\theta) \;=\; m\lambda. \tag{2.39}$$

Equation 2.39 is a more general conclusion compared to Eq.2.31. If the etch depth h is zero, and the incident angle is also zero, then Eq. 2.39 reduces to Eq. 2.31. In other words, Eq. 2.31 is a special case of Eq. 2.39. From Eq. 2.39, it is clear that the direction of the interference maxima depend on the grating constant, diffracted angle, the etch depth, and the index of the grating material.

The grating used in this study is this type of phase generator. However, it is extended into a two-dimensional grating. It is a high efficiency, blaze-like effect binary grating.[40] Figure 2.15 is a diagram of this two-dimensional, two-phase-level grating. The bold outline represents one cell of this grating, and the grating constant d equals the width of a cell. Since each cell of the two-dimensional grating is a square, four equiangular, diverging, and symmetric spectral orders are produced.

1	0	1	0	1	0	1	0
0	1	0	1	0	1	0	1
1	0	1	0	1	0	1	0
0	1	0	**1**	**0**	1	0	1
1	0	1	**0**	**1**	0	1	0
0	1	0	1	0	1	0	1
1	0	1	0	1	0	1	0
0	1	0	1	0	1	0	1

FIG. 2.15. The configuration of the holographic diffraction grating.

In order to understand the design of such a two-dimensional, two-phase-level grating, one enlarged cell is shown in FIG. 2.16. The two phase levels of this grating are represented as level 0 and level 1. It is like a checkerboard, with either all light or all dark squares etched, leaving the other squares unetched. The etch depth is determined by the designed phase difference between the two levels. If an incident wave passes through the grating with zero diffraction angle, the phase difference produced by the etch depth is expressed as

$$\phi = 2\pi h \frac{(n-1)}{\lambda}, \tag{2.40}$$

where n is the refractive index of the diffraction grating, λ is the wavelength of the incident wave, and h is the etch depth. Therefore, if the designed phase difference is π, the etch depth can be calculated as

$$\phi = 2\pi h \frac{(n-1)}{\lambda} = \pi, \tag{2.41}$$

$$h = \frac{\lambda}{2(n-1)}. \tag{2.42}$$
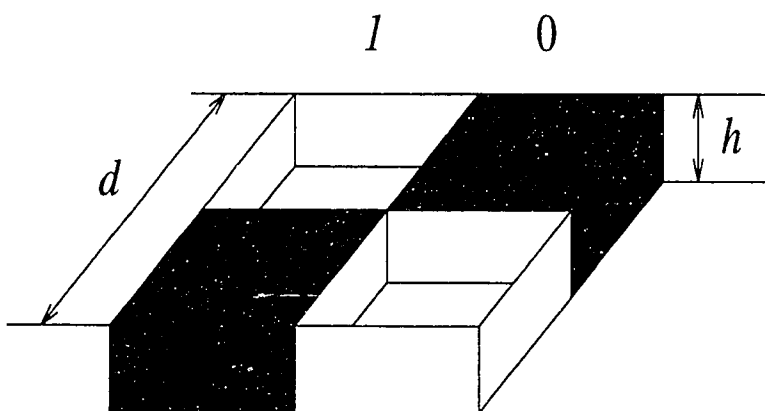
FIG. 2.16. One cell of the diffraction grating.

From Eq. 2.42, the etch depth produces an optical path difference of a half wavelength between the rays passing through the two levels. Therefore, the grating has minimum energy intensity in the norm direction of the grating. In other words, no energy is transmitted in this direction. According to Eq. 2.39, the direction of the first diffraction maximum can be calculated. Since the grating constant d for this grating is 10 microns, the refractive index is 1.475, and the wavelength is 441.57 nm, the θ for $m = 0$ can be obtained by Eq. 2.39, and it is $1.266°$.

2.1.3. The optical system

For this prototype, the optical system which recombines the uniform and coherent beams was eight five degree prisms. Prisms are, essentially, blocks of optical material with flat polished sides which are arranged to be at precisely controlled angles to each other.[41] They can be used in optical system to deviate a beam of light or rotates an image. By rotating the prisms, the four beams were recombined at a focal plane. The recombined beams then were recorded on film. One of these prisms is shown in FIG. 2.17.
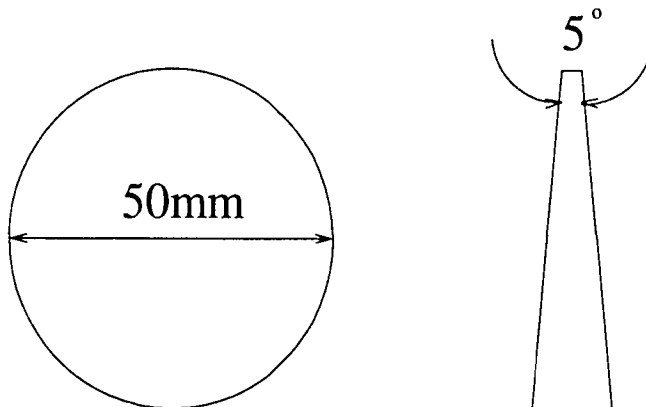
FIG. 2.17. The schematic drawing of a prism of the holographic system.

2.2. The UV laser system of the production model

Since the design and analysis for the prototype established the design theory, a UV laser system which will be used in a production model is designed.

2.2.1. The laser and the expansion system

To achieve a large interference pattern, it is desirable to have a high power laser. In the UV laser projection system, a Coherent Enterprise Model 625 Argon Ion UV laser manufactured by Coherent Inc. will be utilized. This laser has a power of 250 mw. Similar to the prototype, this laser beam will also be expanded before the beam pass through the reshaping system. The beam expansion system is a Newport-Klinger Tropel UV Model T27-100-150 containing a 5 μ pinhole spatial filter. This expander has a power of 66.67x. Since this laser contains two other wavelengths, which are 351.1 nm and 351.2 nm, a narrow bandpass filter (Andover Corp.) will be utilized to separate the 363.789 nm wavelength which is the desirable wavelength due to the sensitivity of the photosensitive material of the substrate. The spectral data of the bandpass filter is shown in FIG. 2.18. The center wavelength of this filter is at 364.265 nm. The transmission for zero angle incident of the center wavelength is 86.34%. The bandwidth is 3.280 nm. It is clear that the 351.1 nm and 351.2 nm wavelengths will be absorbed by this filter.
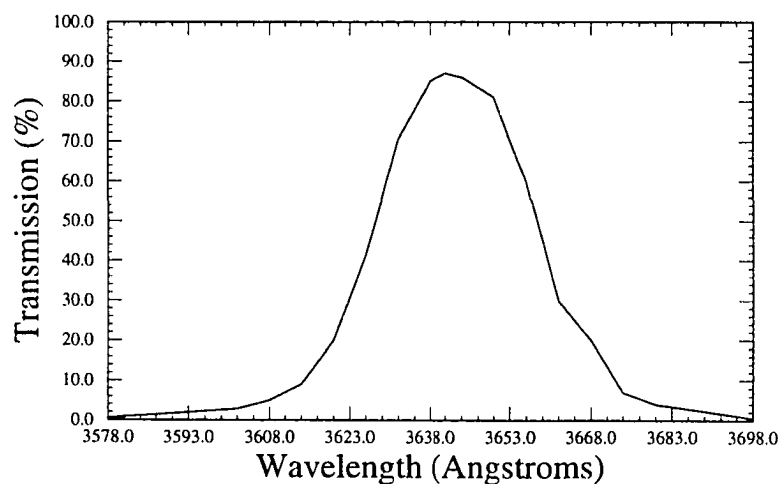
FIG. 2.18. Spectral data of the bandpass filter.

2.2.2. The reshaper

The reshaping system for the UV laser system converts a Gaussian beam profile into a uniform profile while it is expanded into a beam of 80 mm in diameter. Even though it is known that this UV laser has a Gaussian beam profile, the ideal method should be direct measurement of the profile so that the input data of the reshaper is based on the experiment data. Thus, the design error was minimized.

2.2.2.1. The input data. The laser beam after the expansion system has been measured. The measurement data was fitted into a Gaussian using the same method discussed in section 2.1. The fitting result is shown is FIG. 2.19. This beam has a Gaussian distribution with α equal to 9.18 mm.
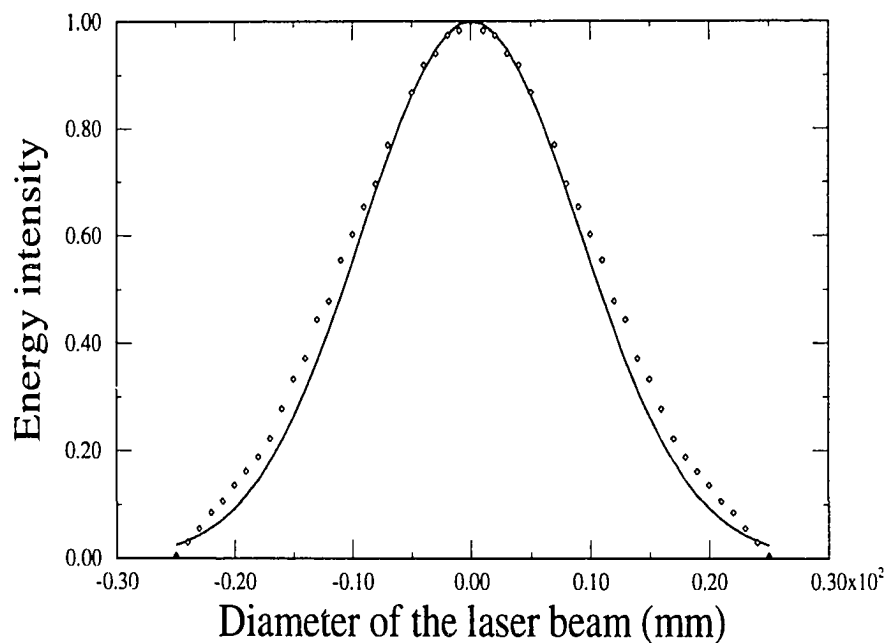
FIG. 2.19. UV laser beam profile at the central cross-section before the reshaper.

Even though this input beam was a Gaussian profile like the prototype, the primary working aperture includes three-sigma of the total energy. According to the previous discussion in this chapter (page 16), the input beam profile can be expressed as

$$\sigma(r) = exp\left((-4.5)\left(\frac{r}{r_0}\right)^2\right).$$ (2.43)

This is due to the fact $r_0 = 3\alpha$. When, $r = r_0$, $\sigma(r_0) = exp(-4.5)$; therefore, 98.89% of the total energy is included in the incoming beam profile.

Based on this input data and the design theory of the reshaping system, two-plano-aspherical lenses were designed to convert the input beam into a uniform profile with a beam diameter of 80mm.

2.2.2.2. The design results. The design theory of this reshaper is same as that of the prototype. The data from the solution of the differential equations were also being fitted into the conventional optical formula:

$$z = \frac{cr^2}{1 + \sqrt{1 - (1 + \kappa)c^2 r^2}} + \sum_{i=2}^{n} A_{2i} r^{2i}.$$ (2.44)

Table 2.3 summarizes the design results of the UV laser reshaper.

Table 2.3. Parameters of a UV laser beam reshaping system

Wavelength = 363.789 nm

Radius of the Working Aperture of the Primary = 27.0 mm

Radius of the Working Aperture of the Secondary = 40.0 mm

Distant Between the Lenses = 500 mm

Surrounding Medium Is Air, Index = 1.0

Thickness of the Two Lenses = 15 mm

Surface Parameters

Lens Surface	Primary	Secondary
Diameters(mm)	100.0	100.0
Vertex Radii(mm)	105.65122	333.54885
Index	$1.44504(CaF_2)$	$1.44504(CaF_2)$
Thickness(mm)	15.0	15.0
Conic Constant	-0.78848	-0.73469
$A_4(mm^{-3})$	-4.61753×10^{-6}	4.50140×10^{-8}
$A_6 (mm^{-5})$	2.00366×10^{-9}	-8.18844×10^{-11}

This system was also analyzed by the flux-flow equation, and the results are shown in FIGs. 2.20 and 2.21.
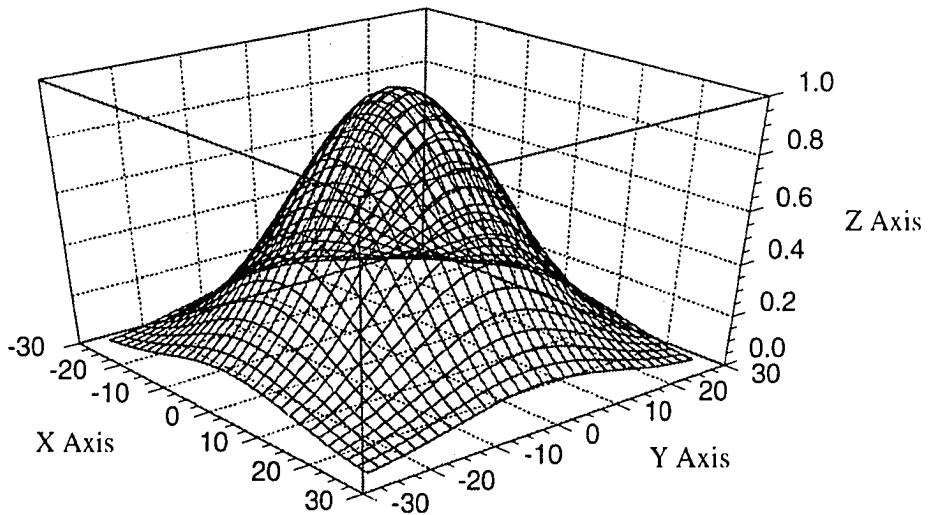
FIG. 2.20. The input beam profile of the reshaper of the UV projection system.
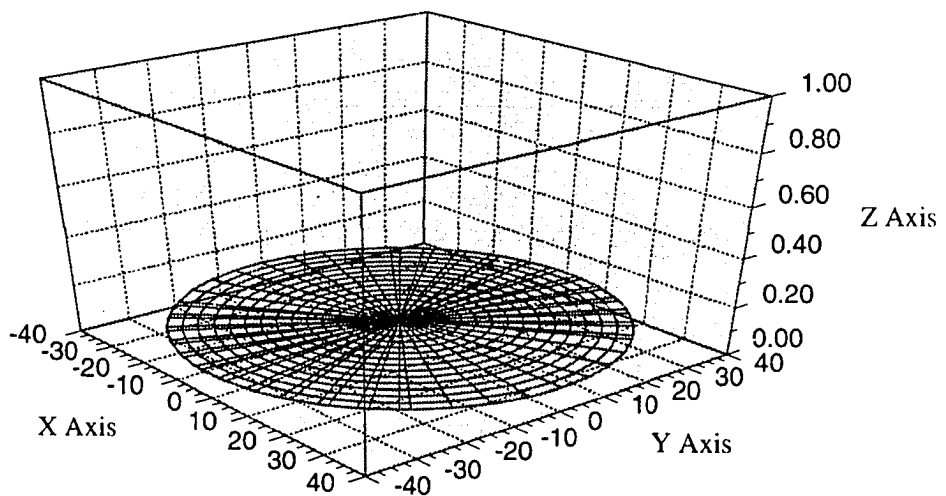
FIG. 2.21. The output beam profile of the reshaper of the UV projection system.

2.2.3. The holographic grating

The binary optics to be used in this system will be a two-dimensional, four-phase-level array generator. Since the shape of each phase level is an equilateral, three diverging and equiangular spectral order beams will be produced. These four phase levels are represent by levels 0, 1, 2, and 3. The phase difference are $0 = 0$, $1 = 2\pi/3$, $2 = \pi$, and $3 = 5\pi/3$. According to Eq. 2.40, etch depths for the different phase level can be calculated as

$$h_0 = 0, \; h_1 = \frac{\lambda}{3(n-1)}, \; h_2 = \frac{\lambda}{2(n-1)}, \; h_3 = \frac{5\lambda}{6(n-1)},$$

where n is the refractive index of the grating, and λ is the wavelength of the incident wave. The multiple beams produced by such a phase grating will create a lattice of hexagonal intensity maxima extending through the photosensitive substrate when the diverging beams are recombined. This phase generator is shown in FIG. 2.22. The bold outline represents one cell of this grating.
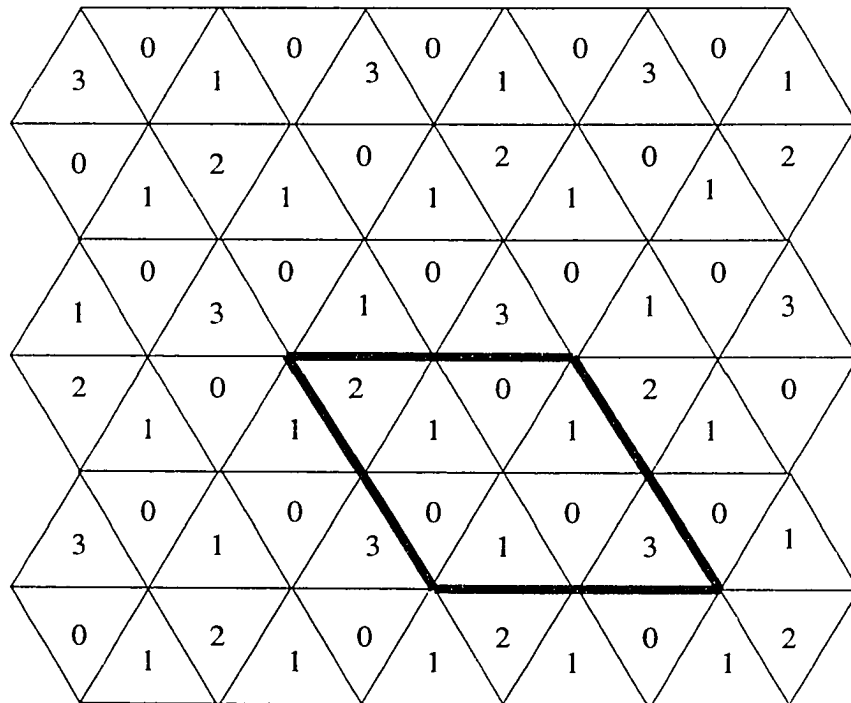
FIG. 2.22. Four-phase-level generator for the UV projection system.

2.2.4. The focusing optical system

The diverging beams produced by the diffraction grating need to be recombined so that the desired interference pattern could be created. Unlike the prototype, this UV laser system uses multiple lenses to recombine the beams instead of the prisms. This lens system includes two parts: objective lens and the tail-end section. [42]

The objective lens system consists of five elements. It is shown in FIG 2.23. Such a five-element object lens system will separate the diverging spectral orders from the phase generator. After passing through this five-lens-element, the diverging beams are separated and focused at individual points on the focal plane of this objective lens system. By using the lens system, the space needed for separating the diverging beams has been reduced. Therefore, the projection system can be made more compact than the prototype. The parameters of this objective lens system are shown in Table 2.4.
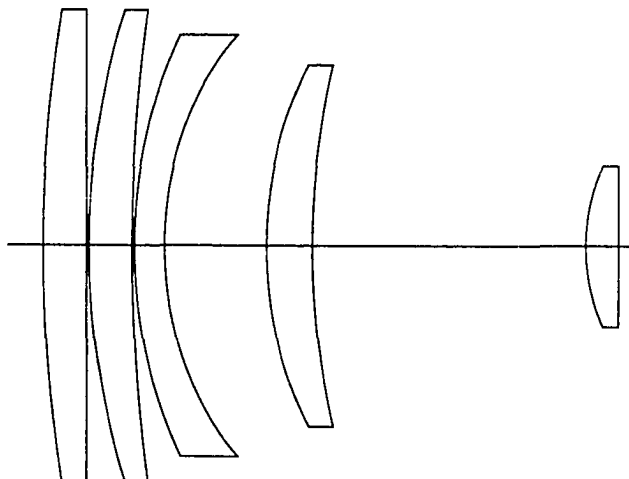
FIG. 2.23. Objective lens of the UV projector.

Table 2.4. Parameters of objective lens system

Surf #	Radius(mm)	Thickness(mm)	Index	Aperture(mm)
1	228.1174	11.517281	1.536451(UBK7)	45.0
2	0	0.635000	1(Air)	45.0
3	120.65000	11.345023	1.536451(UBK7)	45.0
4	267.08100	0.635000	1(Air)	45.0
5	78.30820	8.000000	1.536451(UBK7)	40.0
6	55.49900	26.944376	1(Air)	40.0
7	62.71260	12.315787	1.536451(UBK7)	34.0
8	119.78640	72.504404	1(Air)	32.0
9	29.64180	8.779575	1.536451(UBK7)	14.5
10	0	17.50000	1(Air)	12.5

The focused beams at the focus plane of the objective lens system pass through a six-element tail-end-lens system. This system is designed to correct the off-axis stretching distortion of the standing wave grid pattern, and this correctional system is optimized for a spherical field. These tail-end optics create virtual focal points on a virtual focal plane, as shown in FIG. 2.24. As the interferometric light ray angles from the real focal points, they decrease more and more when they are further off-axis. Since the virtual focal points spread further and further to correct the off-axis distortion, the interferometric angles are kept the same. Otherwise, the smaller the interferometric angles, the bigger the fringe pattern would become, hence the stretching effect toward the edges of the field.

One feature of this particular tail-end correctional lens system design is that not only all of the off-axis interferometric angles are corrected, but also all normal to the three light ray interfering bundles intersect the center point of the virtual focal plane. If

this were not a feature of the design, the channels through the three-dimensional honeycomb-like grid patterns could not normally be used to transmit light rays toward a common point. Also, there would be an effective distortion in the grid pattern at target distances other than that for which the tail-end correctional optics were optimized. The normal may be considered as the bisectors of the angles created only by two interfering light rays in each bundle with its normal. Again, each bisector traces back to intersect the center point of the virtual focal plane. The parameters of this tail-end lens system are presented in Table 2.5.
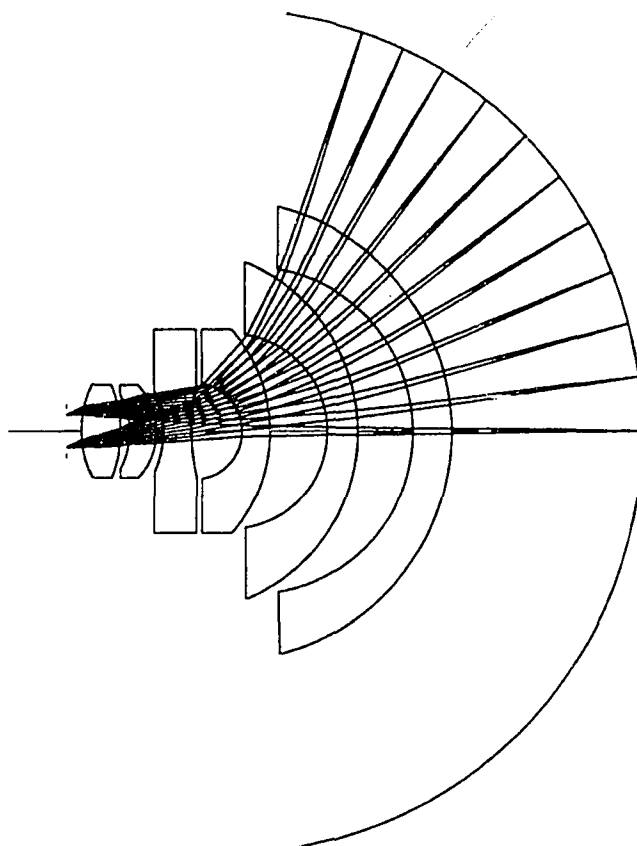
FIG. 2.24. The tail-end section of the UV projector.

Table 2.5. Parameters of tail-end lens system

Surf #	Radius(mm)	Thickness(mm)	Index	Aperture(mm)
1	6.67004	2.538741	1.536451(UBK7)	3.0
2	-7.89432	0.625322	1(Air)	3.0
3	-4.78790	1.823289	1.536451(UBK7)	3.0
4	-4.27228	0.441378	1(Air)	3.0
5	-6.36524	1.800000	1.536451(UBK7)	3.0
6	12.64920	3.370817	1(Air)	3.0
7	-3.09372	1.816353	1.536451(UBK7)	4.0
8	-9.88060	3.712793	1(Air)	6.5
9	-6.28142	2.000000	1.536451(UBK7)	6.5
10	-11.68400	3.605108	1(Air)	10.0
11	-10.50544	2.500000	1.523762(K10)	12.0
12	-14.77010	12.50000	1	15.0
IMG	-27.00000	0.000000	1	30.0

From Table 2.5, it is clear that the image focusing point is at a spherical surface with a radius of 27 mm.

Since the reshaped laser beam is passing through this optical system, it is important to analyze this system so that the uniform beam will not be distorted by such a system. Therefore, this lens system is analyzed by ray tracing equation of GENII-PLUS.[29] If the incoming rays are uniformly distributed, the ray tracing results showed that the outgoing rays at the imaging surface of the optical system are also uniformly distributed. This suggests that this optical focusing system does not change the energy intensity profile. Therefore, a uniform beam coming form the reshaper will be kept uniform at the substrate surface.

2.3. Chapter summary

In this chapter, the design and analysis of the beam reshaping system are presented. Based on conservation of energy and constant optical path length condition, a two-plano-aspherical lens system has been designed. Such a system converts an arbitrary radially symmetric beam profile into a desired output beam profile with high energy efficiency. In this study, a Gaussian beam has been converted into a uniform profile. Theoretical calculations predicted that one reshaper which operates at a particular wavelength can be used to reshape a different wavelength by simply varying the lens spacing. This reshaper is then integrated into a prototype holographic projection system. This projector using a two-dimensional, two-phase-level diffraction grating produces four diverging and symmetric spectral order beams. The derivation of the grating equation of the refractive grating is shown in section 2.1.1. With the experiences gained from the design and testing of the prototype of the reshaping system, a UV laser beam profile reshaping system, which will be used in a production model of the projection system is presented in section 2.2.1. This design is based on the experimental data measured directly form the input beam of the reshaper. After the reshaper, the uniform beam will pass through a two-dimensional, four-phase-level diffraction grating. Such a grating will produce multiple coherent and uniform beams, which interfere to produce desired patterns, such as diverging lattice of hexagonal intensity maxima extending through the photosensitive substrate. The optical system which is used to combine the diverging beams is also given in this section. Since the optical system will couple with the reshaper, its optical performance is also analyzed, and it is presented in the last part of section 2.2.

The design and analysis of the beam reshaping system provide a simple and energy efficient method for beam profile reshaping. Its application to the holographic projection system illustrates that this two-plano-aspherical lens system can contribute to many uniform illumination applications, which are widely used by today's technology.

CHAPTER 3

EXPERIMENTAL METHOD

After the design and analysis, a prototype of the reshaping system and the prototype of the holographic projection system were assembled and tested. Testing results show that the two-aspherical-lens reshaping system effectively converts a Gaussian intensity profile into a uniform beam profile which enhances the performance of the holographic projector. In section 3.1, the results of testing the reshaper will be presented. This includes qualitative testing beam profiles of a Helium Cadmium laser by a camera-film system as well as quantitative testing by a camera-computer-based imaging processing system. The theoretical results from section 2.1.1.4, which predict that different lasers (wavelengths) can be reshaped by one reshaping system when the lens spacing varies correspondingly, was also tested, and the experimental results illustrated that one laser beam reshaper is capable of reshaping multiple lasers by changing the distance between the two aspherical lenses accordingly. Since light of different wavelengths is often used for different applications, it is important to test these theoretical results to determine whether one reshaper can be used for applications using multiple wavelengths. Allowing tolerances of assembling the reshaping system is investigated in section 3.1.2.3. In section 3.2, results of testing the prototype of a holographic projector are reported. Testing results demonstrate that this projector is an effective and compact projection system which produces four uniform and coherent beams without truncating the beams and using mirrors. The projector was also tested with and without the reshaping system. The testing results clearly show that the reshaper enhanced the performance of the projection system and that it is possible to produce

52

monolithic micro-optical arrays over a large area uniformly. Section 3.3 gives conclusions of experimental testing results.

3.1. Testing the prototype of the reshaping system

A prototype of the reshaping system was fabricated, assembled, and tested. The experimental procedures of testing the reshaper included measurements of the beam profiles of a Helium Cadmium laser before and after the reshaping system. These measurements involved testing the Helium Cadmium laser beam profiles qualitatively by a camera-film system and quantitatively by a camera-computer system. The testing results show that the two-plano-aspherical lens system reshaped the HeCd laser beam profile from a Gaussian beam into a more uniform beam profile. According to the theoretical results predicted in Chapter 2 that one beam reshaper is capable of reshaping a different laser wavelength by simply varying the distance between the two lenses, a beam profile of a Helium-Neon laser of wavelength of 632.8 nm was reshaped to test the reshaping system, which was designed for the Helium Cadmium laser of 441.57 nm. Allowing assembling tolerances, such as tilting and decentering the lenses, were also investigated. This testing system is shown in FIG. 3.1.

3.1.1 The experimental setups of the testing system

This testing system consists of a laser, an expansion system, the reshaper, and a detector system, which either is a 35 mm camera for qualitatively testing or a camera-computer system with image processing software for the quantitatively testing.

3.1.1.1. The laser. The laser used in this prototype is a Class III b Helium Cadmium laser with wavelength of 441.57 nm. It has a power of 25 mW. Its diameter for the width of 1/ e^2 is 1 mm. The divergence of this laser is 0.6 mrad.

Expansion system

HeCd laser

Spatial filter

Primary

Secondary

Personal computer

Panasonic video camera
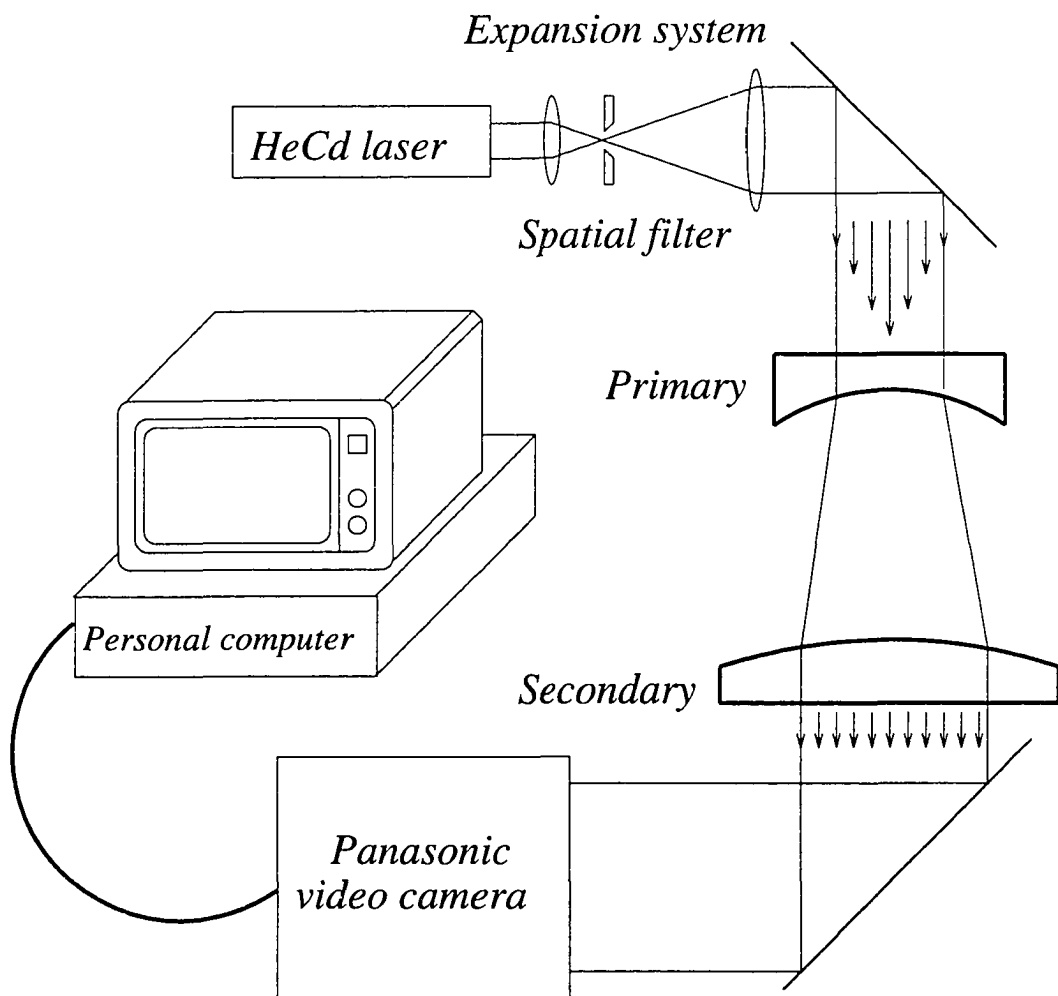
FIG. 3.1. The testing system.

3.1.1.2. The expansion system. The lens system was designed to reshape a Gaussian incoming beam with a diameter of 16 mm. Since the laser beam has a diameter of 1 mm for the $1/e^2$, it needed to be expanded by a factor of 16. An optical system was used to expand the laser beam. It is shown in FIG. 3.2. This system consists of two elements: input and output units. The input includes two lenses with a focal length f_1, and the

output is also a doublet with focal length f_2. From the geometrical optics,

$$\frac{d}{D} = \frac{f_1}{f_2};$$
(3.1)

therefore,

$$D = \frac{f_2}{f_1}d.$$
(3.2)

For this expansion system, $d = 1$mm, $f_1 = 6$mm, and $f_2 = 100$mm. Therefore,

$$D = \frac{100mm}{6mm} \times 1mm = 16.67mm.$$
(3.3)
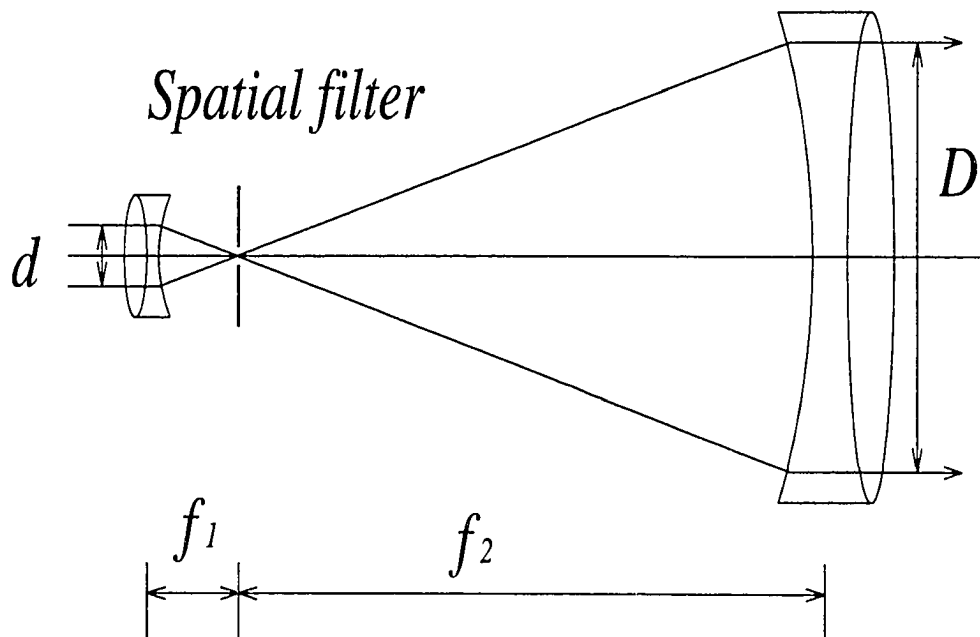
FIG. 3.2. The expansion system.

A spatial filter was placed at the focal point of the expansion system to eliminate the high order noise. According to the diffraction theory,[43] the diameter of the pinhole can be calculated based on the laser parameters:

$$D = F\left(\frac{1.2\lambda}{d} + \theta\right),$$

(3.4)

where d = beam diameter at $1/e^2$; F = focal length of focusing optics (f_1 of the expansion system in this study); λ = laser wavelength; θ = divergence of laser. Substituting the values of these parameters, the pinhole size can be obtained:

$$D = 6 \cdot \left(\frac{1.2 \cdot 441.57 \cdot 10^{-6}}{1} + 0.6 \cdot 10^{-3}\right) = 6.8 \text{ microns.}$$

(3.5)

Most available commercial pinholes are 5 μ, 6 μ, and 8 μ. Since the Newport/ Klinger did not have a 6 μ pinhole in storage, a 5 μ pinhole was placed inside this spatial filter. Since it was slightly smaller than the designed pinhole, a 10 μ pinhole was used to test whether or not it would work. As expected, a 10 μ pinhole did not eliminate the high order noise. Therefore, a 5 μ pinhole was chosen to be used in these testing experiments.

3.1.1.3. The lenses. The two aspherical lenses of this reshaping system were fabricated by Janos Technology Inc. of Townshend, Vermont and are shown in FIG. 3.3. The material is CaF_2, and these two lenses are made by the single diamond point lathe. The primary is a plano-concave asphere, and the secondary is a convex-plano asphere. Since the manufacturer could not promise the surface accuracy after they polish the lenses, initially, the lenses were analyzed before polishing. Therefore, grooves on the surfaces produced by the single point diamond lathe could be seen clearly. Then, the two lenses were sent back to the manufacturer to be polished. The testing results presented in this study are from the polished lenses system.
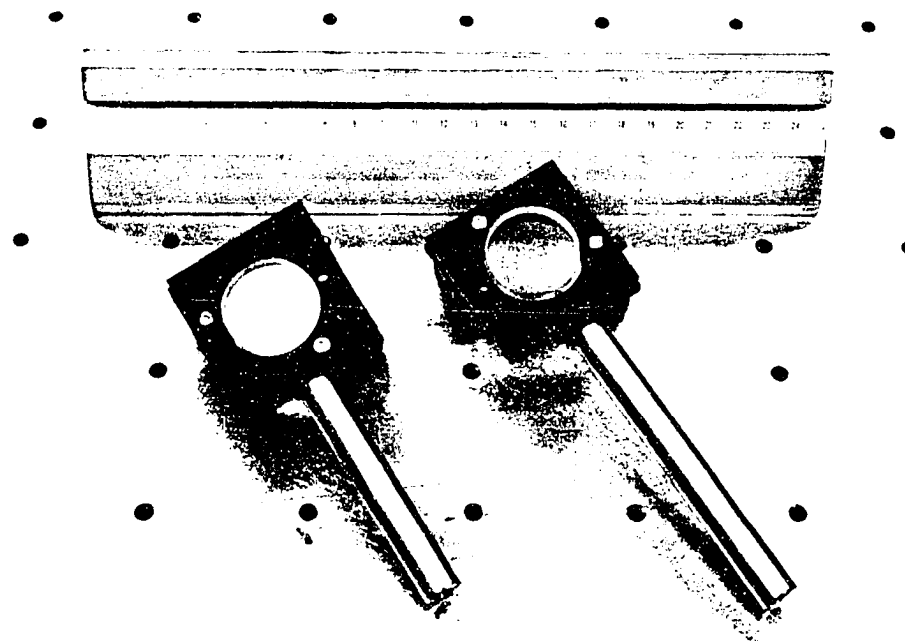
FIG. 3.3. The two aspherical lenses.

3.1.1.4. The camera. In the qualitative testing setup, a Nikon 2000 camera, whose lens has been removed, was used to directly capture the beam profiles. The film used to record the energy intensity was Kodak TMAX 400. In the quantitative testing setup, a Panasonic TV camera (Model WV - 1800) was used to receive the laser beam before as well as after the reshaping system to determine the profiles. This camera was mounted on a translation stage in order to scan the laser beam. By scanning the image, two difficulties were overcome. One was that the laser beam spot was greater than the sensing surface of the camera. Therefore, it was impossible to record the entire image of the laser beam at one time. The other consideration was the nonlinear response of the camera. Since the TV camera was mounted on the translation stage, only one point in the camera field was used. Therefore, the energy profiles were not affected by the non-linearity of the camera field.

3.1.1.5. The personal computer. A Macintosh (Model II) computer, which was connected to the camera, was used to analyze the image of the reshaping system. It is supported by a public domain image processing software - NIH Image 1.44. [44] It can acquire, display, edit, enhance, analyze, print, and animate images. Therefore, when a laser beam from a camera is sent to the computer, it records the image. The image also can be displayed on the computer screen. The quantitative values of the irradiance profiles of as a function of spatial dimension were recorded and read for image analysis.

3.1.1.6. The assembling of the reshaping system. The laser, expansion system, the two aspherical lenses, and the camera were assembled on the same optical rail. The lenses were mounted with lens holders while the holders were mounted on translation stages. The distance between the two vertexes of the aspherical surfaces was 150 mm. The laser was expanded into a 25 mm diameter beam while the energy intensity profile was reshaped from the Gaussian profile into a uniform beam profile. With such a setup, the input and outgoing energy profiles of the reshaping system were recorded. The results of both qualitative and quantitative experiments verified the theory of the beam profile reshaping system.

3.1.2. Testing results of the prototype of this reshaping system.

After assembled the two lenses, a HeCd laser was used to test the performance of this reshaper. Experiments showed that this reshaping system converts a Gaussian beam into a uniform beam profile, which illustrated the design theory in Chapter 2. The testing of the reshaping system also involved testing a HeNe laser to established the theory that a beam reshaper can be used to reshape a different laser wavelength. The investigation of allowing tolerance of this reshaping system is also presented in this section.

3.1.2.1. Testing the reshaper. The testing results of the reshaper by the HeCd laser are presented in this section. The incoming and outgoing profiles of the reshaper were tested both qualitatively and quantitatively.

3.1.2.1.1. Testing the reshaper qualitatively by a camera-film system. The incoming and outgoing beam profile of the reshaper was qualitatively captured by the Nikon 2000 camera. The lens was removed so that the energy intensity profiles were directly recorded on the film. The film was TMAX 400 of Kodak. The exposure time for the Gaussian beam profile was 1/125 second, and the time for the uniform profile was 1/30 second. The reason different exposure times were used for the Gaussian and the uniform is that the uniform beam profile has energy intensity about 1/5 of the center energy intensity of the Gaussian beam profile. To use fully the resolution of the film, it is reasonable to use different exposure times. The films were developed, and the results are shown in FIGs. 3.4 and 3.5.
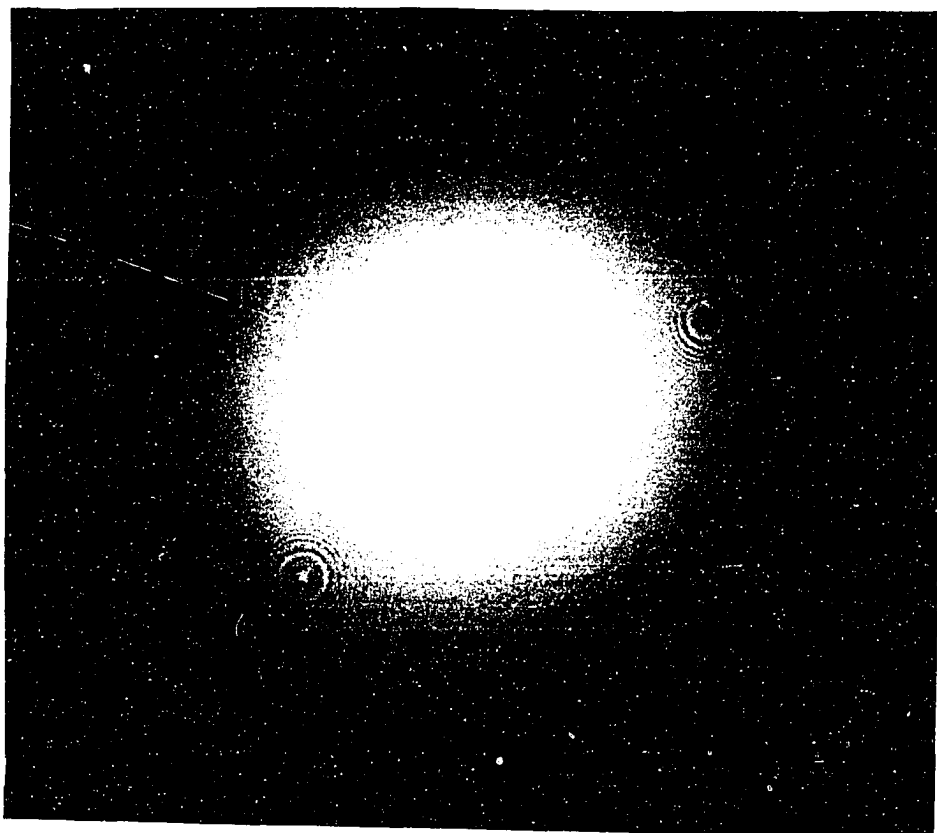
FIG. 3.4. The input energy intensity profile of the reshaper.

Figure 3.4 shows clearly that the center has a more intense energy concentration than the edge. This is expected since this is a Gaussian distribution.

Figure 3.5 shows the output energy intensity profile of the reshaping system. It is obvious that the profile is much more uniform than that of the Gaussian. The rings on the figure are due to the reflected rays from the two aspherical surfaces since no anti-reflection coatings were used for these two lenses.

FIG. 3.5. The output energy profile intensity of the reshaper.

3.1.2.1.2. Testing the reshaper quantitatively by a camera-computer system. The incoming beam profile and the outgoing beam profile of the reshaping system were also recorded quantitatively by a camera-computer system. The Panasonic TV camera was used to scan the laser beam across its diameter. The results are shown in FIG. 3.6. The diamond dots represent the input profile, and the Gaussian-like solid line is the fitted curve of the incoming data (see Appendix B). The solid diamond dots represent the outgoing beam profile of the reshaper, and the horizontal solid line is the theoretical value for the outgoing beam. These quantitative results clearly demonstrate that the incoming beam, which is a Gaussian beam, has been reshaped into a more uniform irradiance profile. However, manufacturing errors of the lenses deviate the outgoing beam from the ideal uniform beam so that the outgoing beam profile was not perfectly uniform. Nevertheless, the theory that a two-plano-aspherical lens system converts a collimated incoming beam into a uniform output beam has been established.
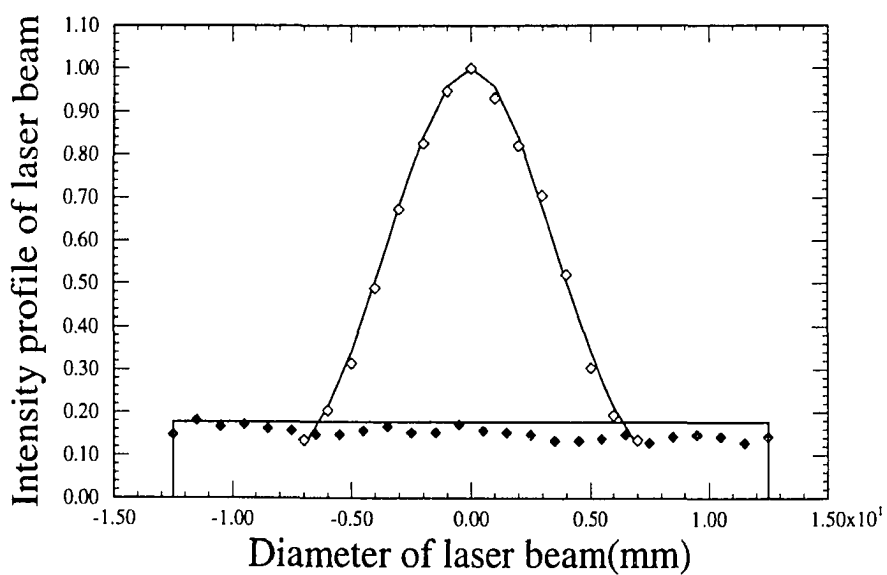

FIG. 3.6. The input and output energy of the lens system.

3.1.2.2. Testing for a different laser wavelength. The prediction that a reshaping system can be used with lasers of different wavelengths by simply varying the lens spacing was tested. In this experiment, a Helium Neon laser with a wavelength of 632.8 nm was reshaped. The testing procedure was based on the calculations in section 2.1.1.4. Therefore, the lens spacing was changed from 150 mm into 152.2 mm. The experimental results in FIG. 3.7 show that the outgoing beam profile is a more uniform beam profile, and the results are similar to the results of the HeCd laser. The diamond dots represent the incoming profile, and the solid diamond dots represent the outgoing beam profile of the reshaper. This result gives a significant impact on many applications. Because materials have different sensitivities to light wavelengths, different applications require different wavelengths. Therefore, these predications and experimental results provide evidence that one reshaper can be applied to multiple applications when different laser wavelengths are used.
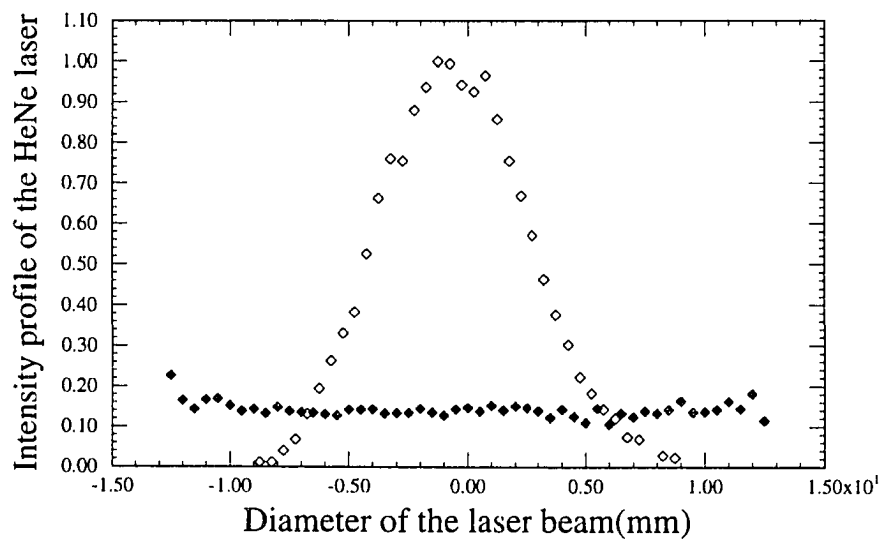
FIG. 3.7. The testing result for the HeNe laser by the same reshaper.

3.1.2.3. Study of allowing assembly tolerances. It is important to understand acceptable assembly tolerances of this reshaper so that the outgoing beam profile will not be distorted by improper assembly. In this study, the lenses of the reshaper were tilted and decentered, and the experimental results showed that this reshaping system is a very stable system. The general university lab environment is suitable for this system. The experiments included tilting the primary lens in 1 degree, tilting the secondary in 1 degree, tilting both lenses 1 degree in the same direction, and tilting both lenses 1 degree in opposite directions. The primary lens decentered 1 millimeter from the center was also tested.

The testing results of the primary lens tilted 1 degree is shown in FIG. 3.8. The energy of the outgoing beam profile has been shifted toward the direction of the tilting. However, the 1 degree assembly error was obvious, and it could be controlled.
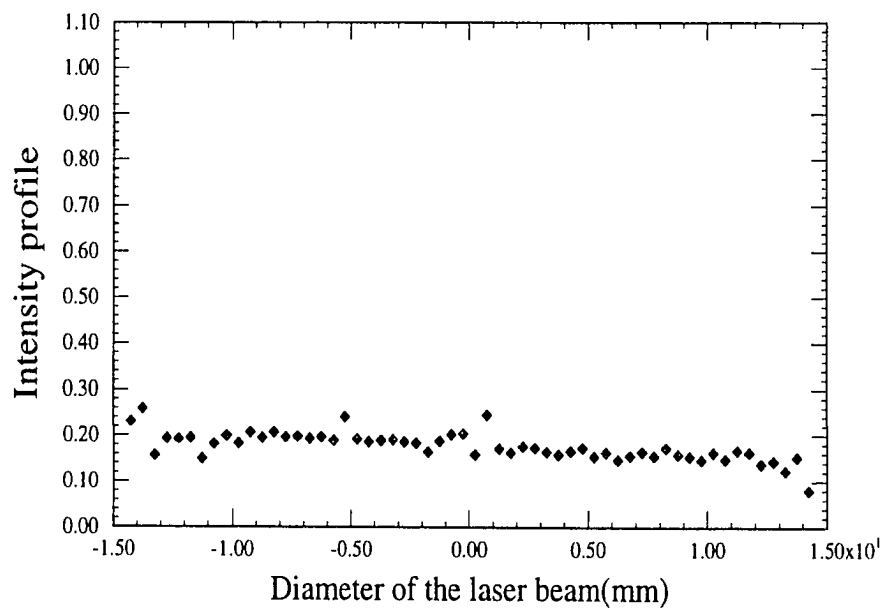
FIG. 3.8. The outgoing energy profile when the primary is tilted 1 degree.

Similarly, the secondary lens was also tilted 1 degree, and the outgoing profile was recorded. The outgoing results were similar to the results of tilting the primary, and it is shown in FIG. 3.9. Again, the energy was shifted toward the tilting direction; however, the situation in which the secondary was tilted 1 degree was avoidable.
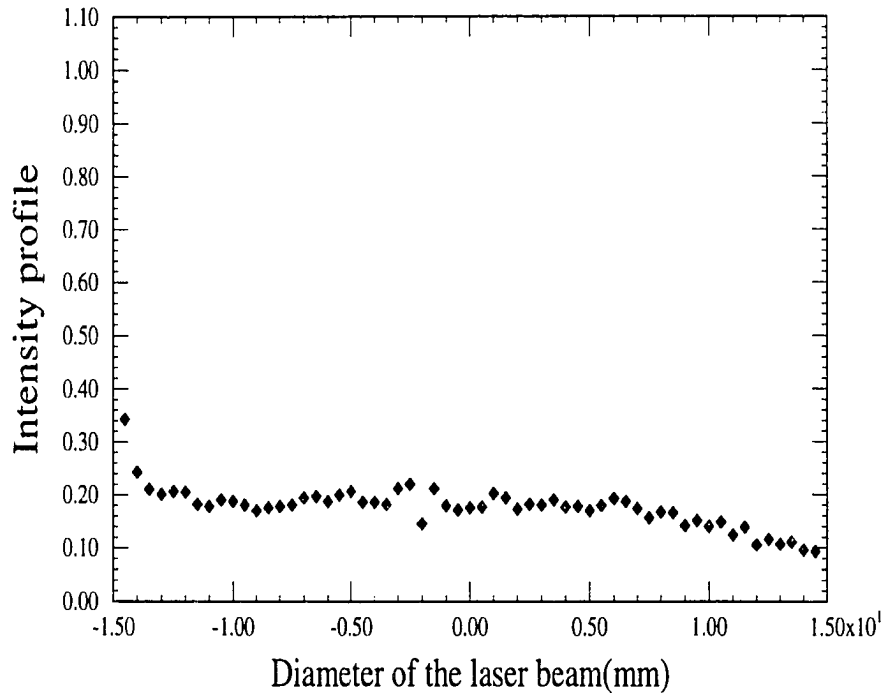
FIG. 3.9. The outgoing energy profile when the secondary is tilted one degree.

Both lenses tilted 1 degree in the same direction was also tested, and the outgoing beam profile is recorded in FIG. 3.10. The outgoing beam profile remained more uniform than when only one lens was tilted. This suggests that it is important to use one fixed mounting system for both lenses rather than mounting them individually.
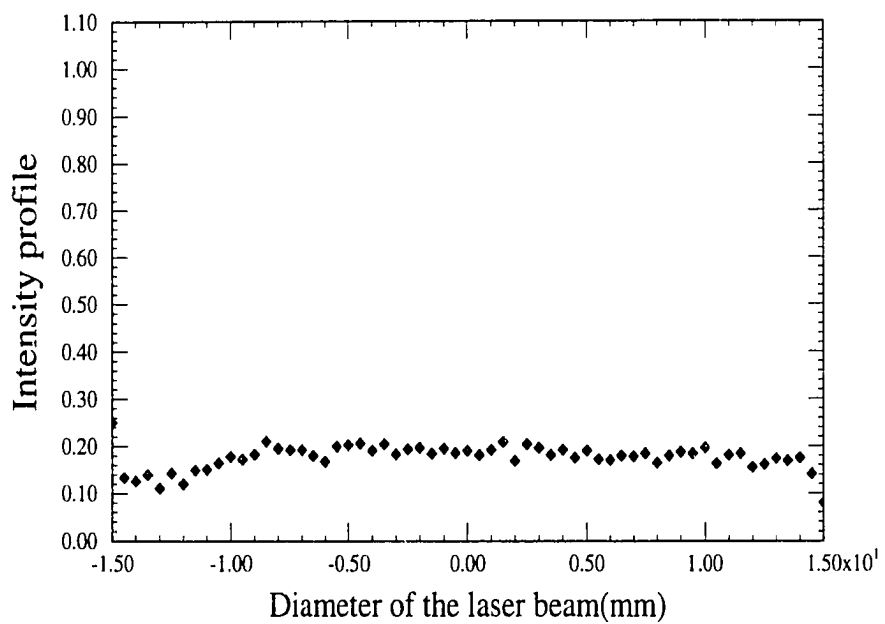
FIG. 3.10. The outgoing energy profile when both lenses are tilted 1 degree in the same direction.

By way of contrast, both lenses tilted 1 degree in opposite directions was also tested. The outgoing energy profile is shown in FIG. 3.11. It is clear that the outgoing energy is much more distorted than in any of the other experiments. Therefore, when both lenses are tilted in opposite directions, the largest distortion of the output beam is obtained.
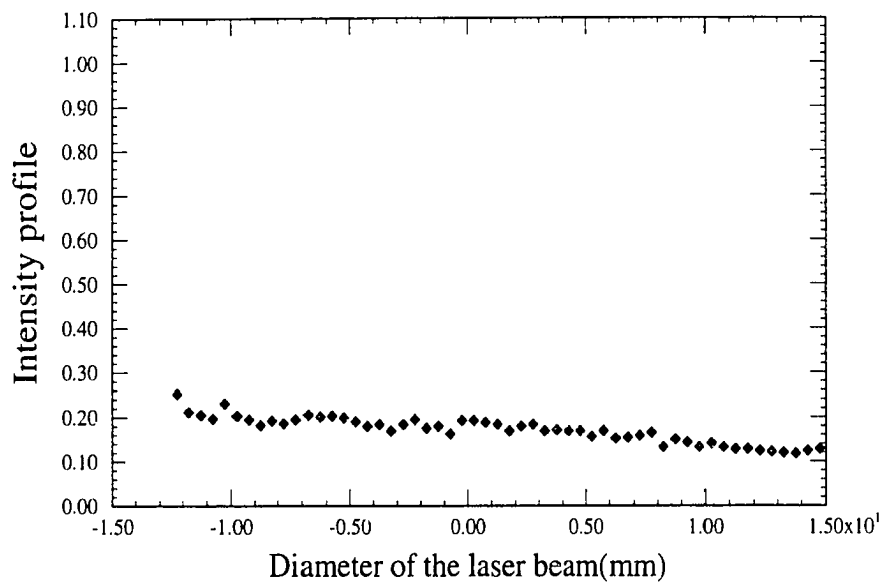
FIG. 3.11. The outgoing energy profile when both lenses are tilted 1 degrees in opposite directions.

The effect of the decentered lens was also investigated. The primary lens was decentered 1 mm from the center. The testing results of the outgoing beam is shown in FIG. 3.12, which indicates that the decentering effect is also not a very sensitive factor for this system.

These experimental results conclude that these two-aspherical lens system is a stable system. Small assembling errors are acceptable; however, tilting two lenses in opposite directions should be avoided.
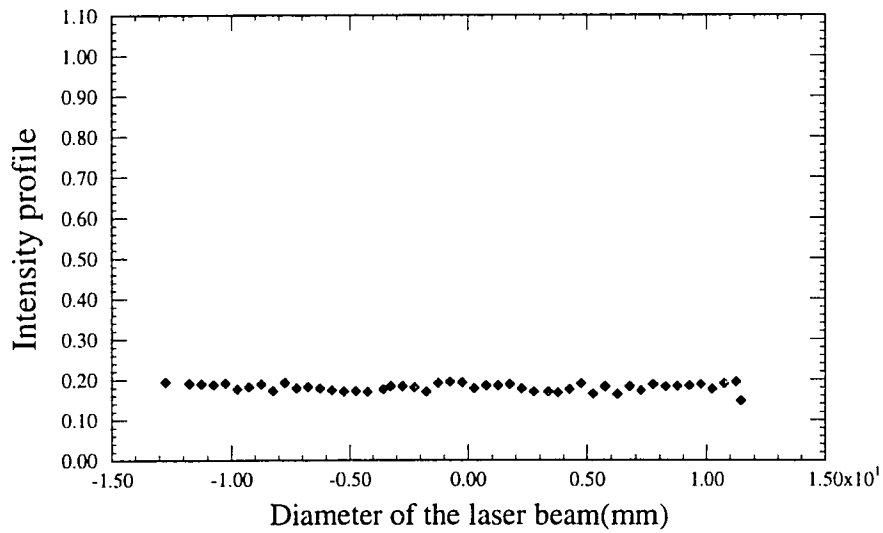
FIG. 3.12. The outgoing energy profile when the primary lens is decentered one millimeter.

3.2. Testing a prototype of the holographic projection system

The testing of the prototype of the holographic projection system was an extension and application of the testing of the reshaping system. In this section, the testing results of this projector are presented. It includes testing the projector by recording the interference patterns on films and comparing the interference grid patterns of the projector with and without the reshaper. The experimental results demonstrate that this projector which uses a beam reshaping system and a holographic diffraction grating is an effective and compact system. Further developments of a holographic projections system, which are beyond the scope of this dissertation, would involve using these interference patters on flat and curved substrates to figure micro-optical arrays, using photosensitive chemical films on the substrates.

3.2.1. Experimental setup.

The setup of this system is shown in FIG. 3.13. This setup was the extension of the experimental setup of the reshaping system. A diffraction holographic grating was placed behind the reshaper, and then eight prisms were assembled to recombine the four beams.
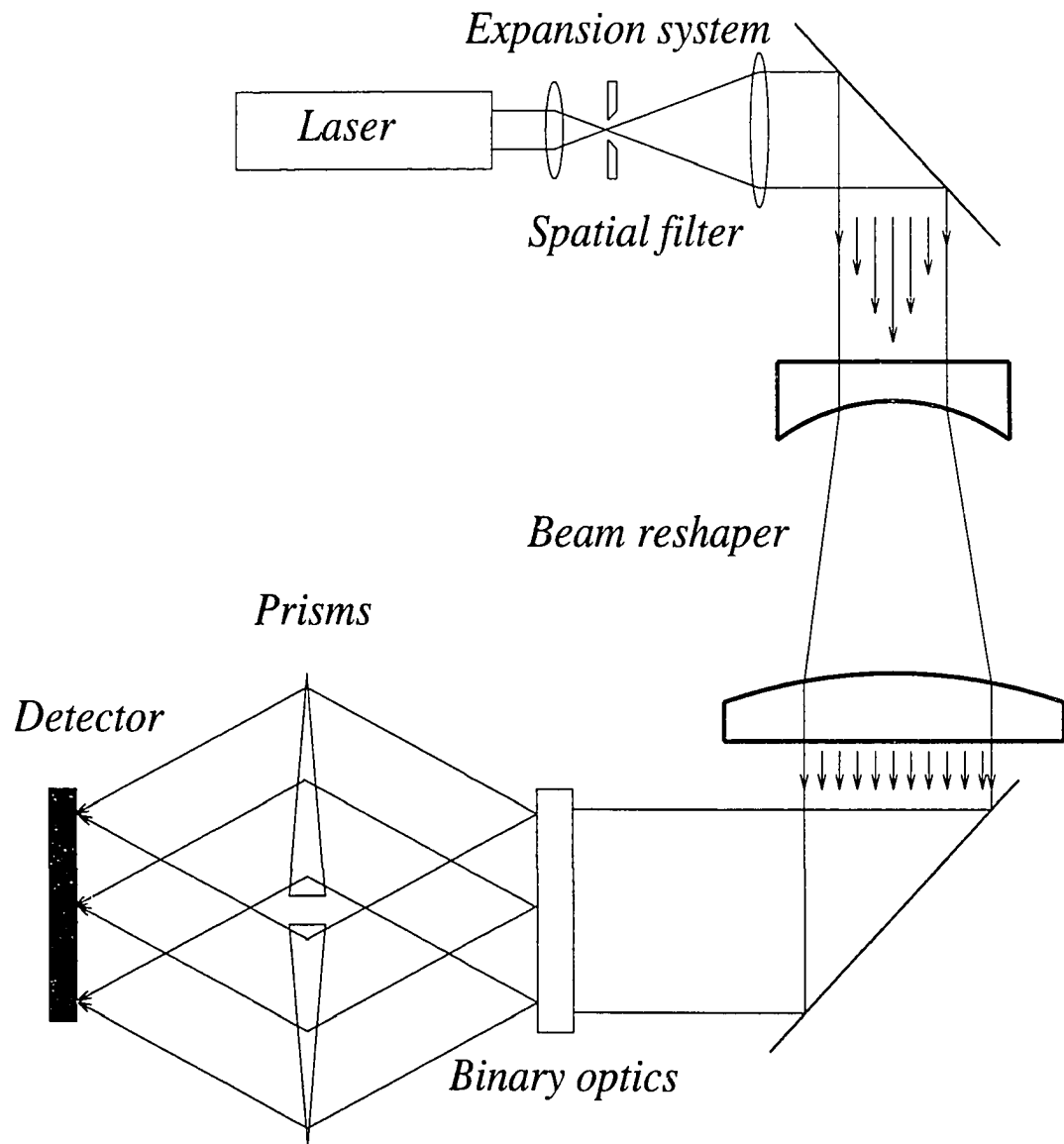
FIG. 3.13. The experiment setup of the prototype of the holographic projector.

69

The eight prisms were mounted on a holder which was built in the Department of Physics shop. Each pair of the prisms were placed face to face. When they were rotated, the beams would rotate accordingly so that the four diverging beams recombined together at a focal plane. The holder of the prisms is shown in FIG. 3.14.
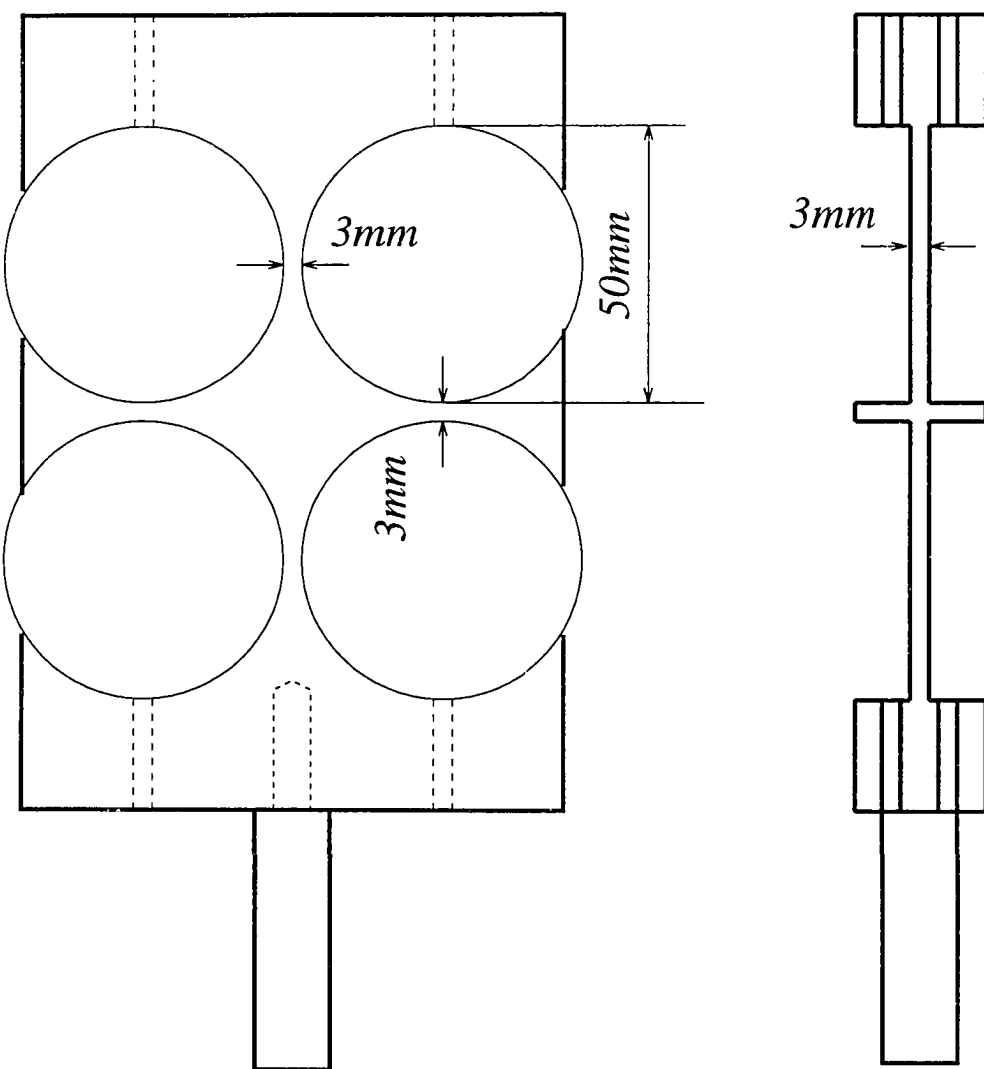
FIG. 3.14. The holder for the eight prisms.

3.2.2. Testing results of the prototype of the holographic projector

With this setup, this projector was tested, and the results are shown in FIG.3.15. The grid size of the interference pattern was calculated (see Appendix C), and the distance between two energy maxima is 25 microns. Experimental measurement by a microscope agreed with the calculations. For a 25 mm diameter beam, there were a thousand energy maxima grids in one diameter of the interference patterns. In this experiment, it is very important to align the holographic grating and the prisms in parallel precisely. Otherwise, there were diffraction lines across the patterns.
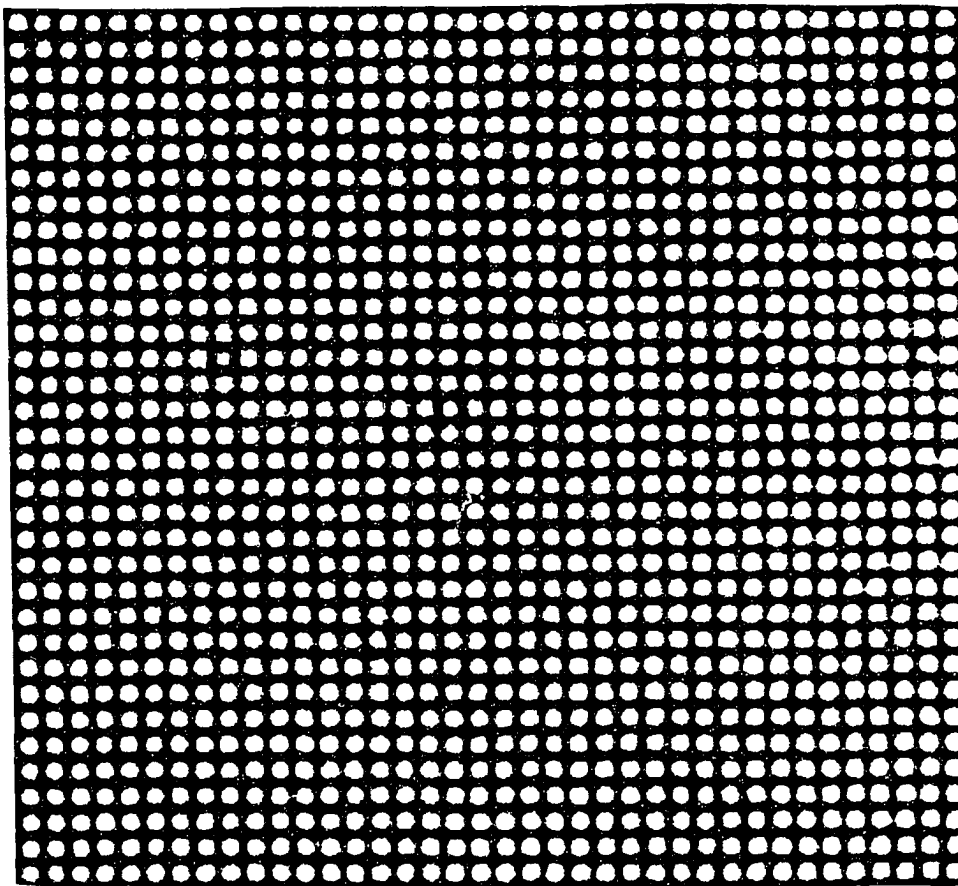
FIG. 3.15. The four-beam interference pattern of the projector.

3.2.3. Comparing the results with and without the beam reshaping system

Experiments were developed also to compare the interference patterns between systems with and without the reshaper. The comparison was among four 1 mm^2 areas which were located at the centers and the edges of the Gaussian and the uniform beam profiles. Since one pair of the grid was 25 microns, there were 40x40 pairs of the grid pattern in the tested areas. Prior to the experiment, the energy of the four areas was calculated. Assuming the origins of the x-y coordinates were at the centers of the beam profiles, the energy would be the integral from -0.5 mm to 0.5 mm in both x and y coordinates for the center areas. For the edge areas, the x was from 6.5 mm to 7.5 mm and y from -0.5 mm to 0.5 mm for the Gaussian, and x was from 11 mm to 12 mm, y from negative 0.5 mm to 0.5 mm for the uniform profile. Based on these parameters, calculations were done to determine the energy at the centers and the edges for both Gaussian and the uniform beam profiles. These are shown in FIG. 3.17.
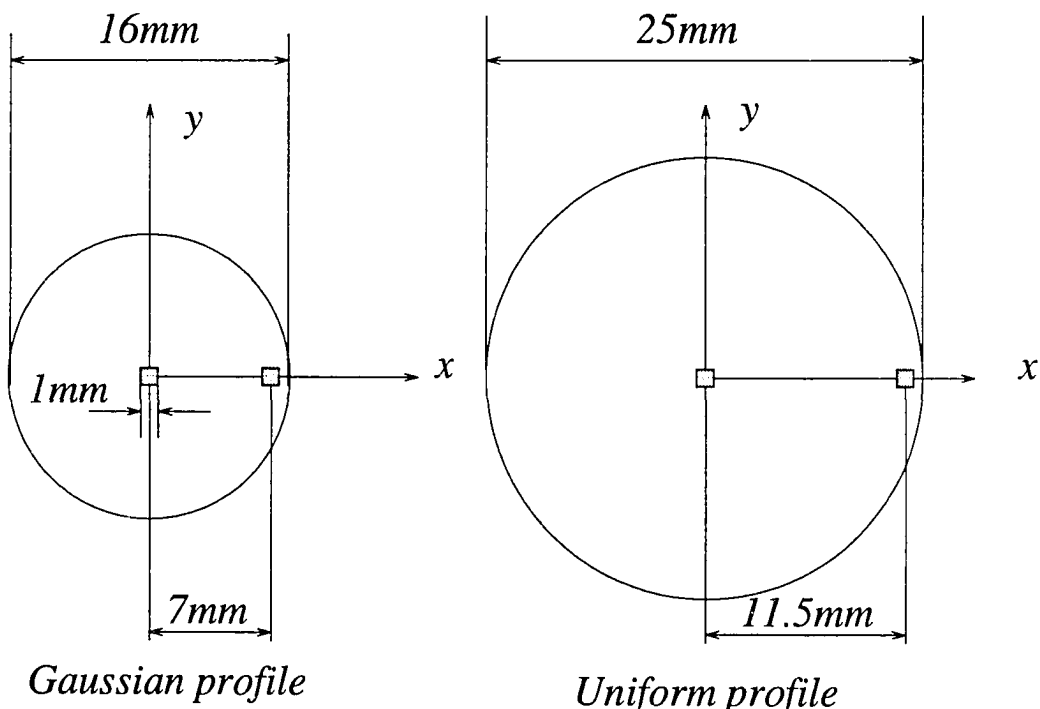
FIG. 3.16. Schematic drawings for the calculations.

For the uniform beam profile, the intensity was 0.177 units (Eq. 2.3 of page 15) on the whole surface. Therefore, the center energy in the 1 mm² area was calculated as

$$E_{UC} = \int_{-0.5}^{0.5} \int_{-0.5}^{0.5} (0.177)\, dxdy = 0.177\, units, \tag{3.6}$$

and the energy at edge was also obtained by the following:

$$E_{UE} = \int_{-0.5}^{0.5} \int_{11.0}^{12.0} (0.177)\, dxdy = 0.177\, units. \tag{3.7}$$

Equations 3.7 and 3.8 show that the energy passing though over 1 mm² test area at the center and the edge was equal for the uniform beam profile as expected.

For the Gaussian beam profile, the energy passed though 1 mm² test area in the center of beam was calculated as

$$E_{GC} = \int_{-0.5}^{0.5} \int_{-0.5}^{0.5} exp\left((-2) \left(\frac{x^2 + y^2}{r_0^2} \right) \right) dxdy = 2.25\, units, \tag{3.8}$$

where r_0 was the working aperture of the primary, which was 8 mm.

Similarly, the energy passed though the 1 mm² area at the edge for the Gaussian was also calculated

$$E_{GE} = \int_{-0.5}^{0.5} \int_{6.5}^{7.5} exp\left((-2) \left(\frac{x^2 + y^2}{r_0^2} \right) \right) dxdy = 0.28\, units. \tag{3.9}$$

Comparing Eqs. 3.8 and 3.9, the irradiance in the center was 8.15 times greater than that at the edge, while the uniform beam had the same irradiance over the entire surface. Therefore, for a large area, a constant irradiance can more readily be achieved when using a uniform input beam than Gaussian beams.

Based on these calculations, corresponding experiments were done. The testing results are shown in FIGs. 3.17, 3.18, 3.19, and 3.20. Figure 3.17 shows the interference pattern of Gaussian at the center, and FIG. 3.18 shows that at the edge area. Both pictures were taken with the same exposure time, which was 4 minutes. The developing time for both films was also the same. Compared with these two figures, it is obvious that the two patterns had different energy intensities, which was a severe degradation in the quality of the interference patterns. On the other hand, the energy intensities at the center (FIG. 3.19) and edge (FIG. 3.20) of the uniform beam profile were very similar. Both FIGs. 3.19 and 3.20 had the same exposure time of eight minutes, and the developing time for films were also the same. The exposure times for the Gaussian beam and the uniform were different because the uniform beam profile was expanded into 25 mm in diameter; therefore, the energy intensity was 17.7% of the center energy intensity of Gaussian. To observe the interference clearly, the exposure time for the uniform beam was twice as long as the Gaussian beam profile. From FIGs 3.17 to 3.20, it follows that the quality of the interference pattern was greatly improved by using the beam profile reshaping system.

3.3. Summary of experimental results

The experimental results of testing the reshaping system by the HeCd laser gave evidence that a two-plano-aspherical lens system can be built to effectively convert a Gaussian beam profile into a uniform beam profile. Since it only consists of two aspherical lenses, it is a rather simple system. The tolerance analysis demonstrated that the reshaping system is a stable system, and requirements for the laboratory environment are not sophisticated. The experimental results of testing the reshaping system with a HeNe laser demonstrated that, by changing a small amount of the lens spacing of the reshaper, one reshaping system which is designed to operate at a specific wavelength can be used to reshape a different wavelength. The testing results of the prototype of the holographic projection system illustrated that the utilization of a beam
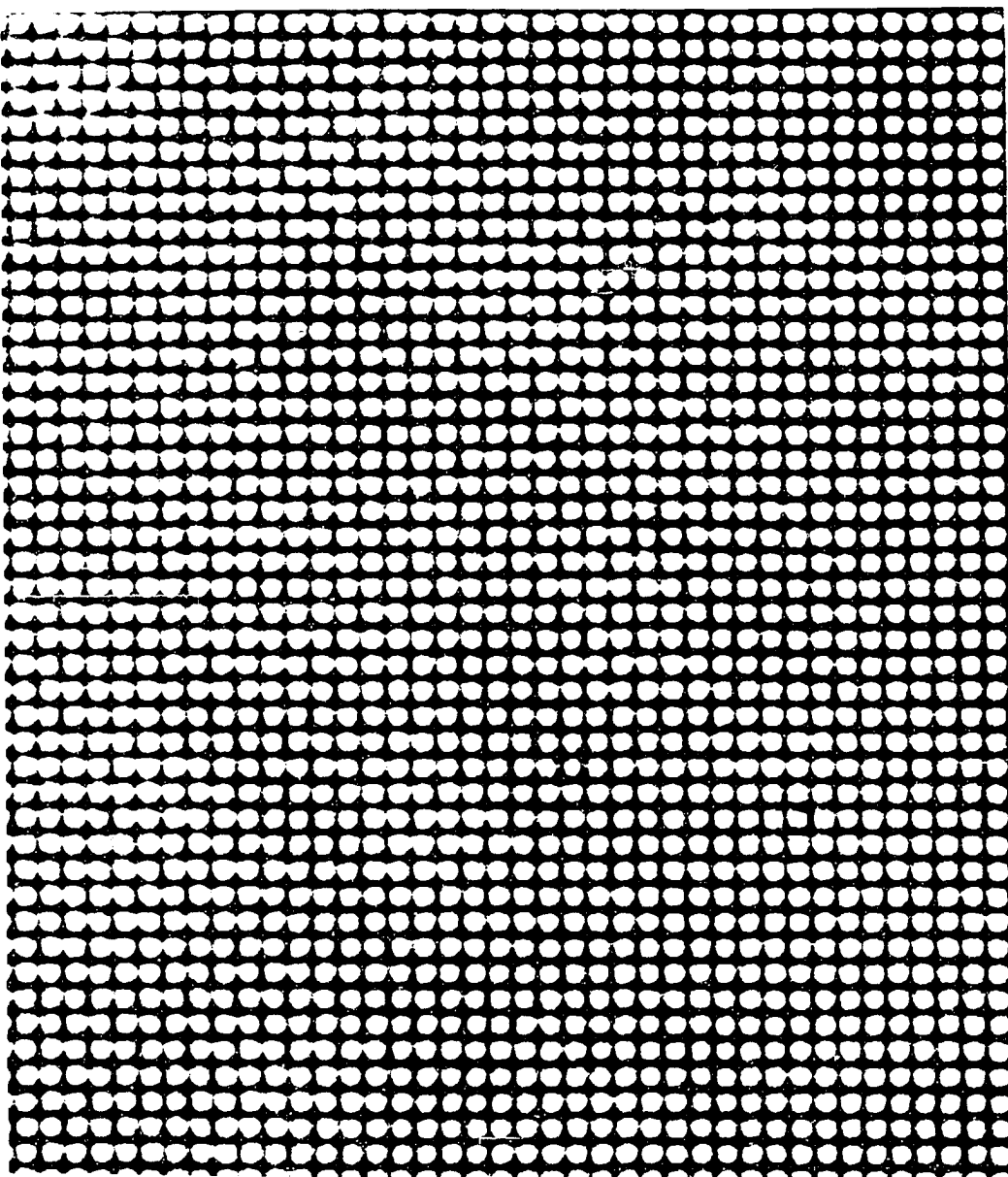
FIG. 3.17. Interference pattern at the center of the Gaussian beam profile.
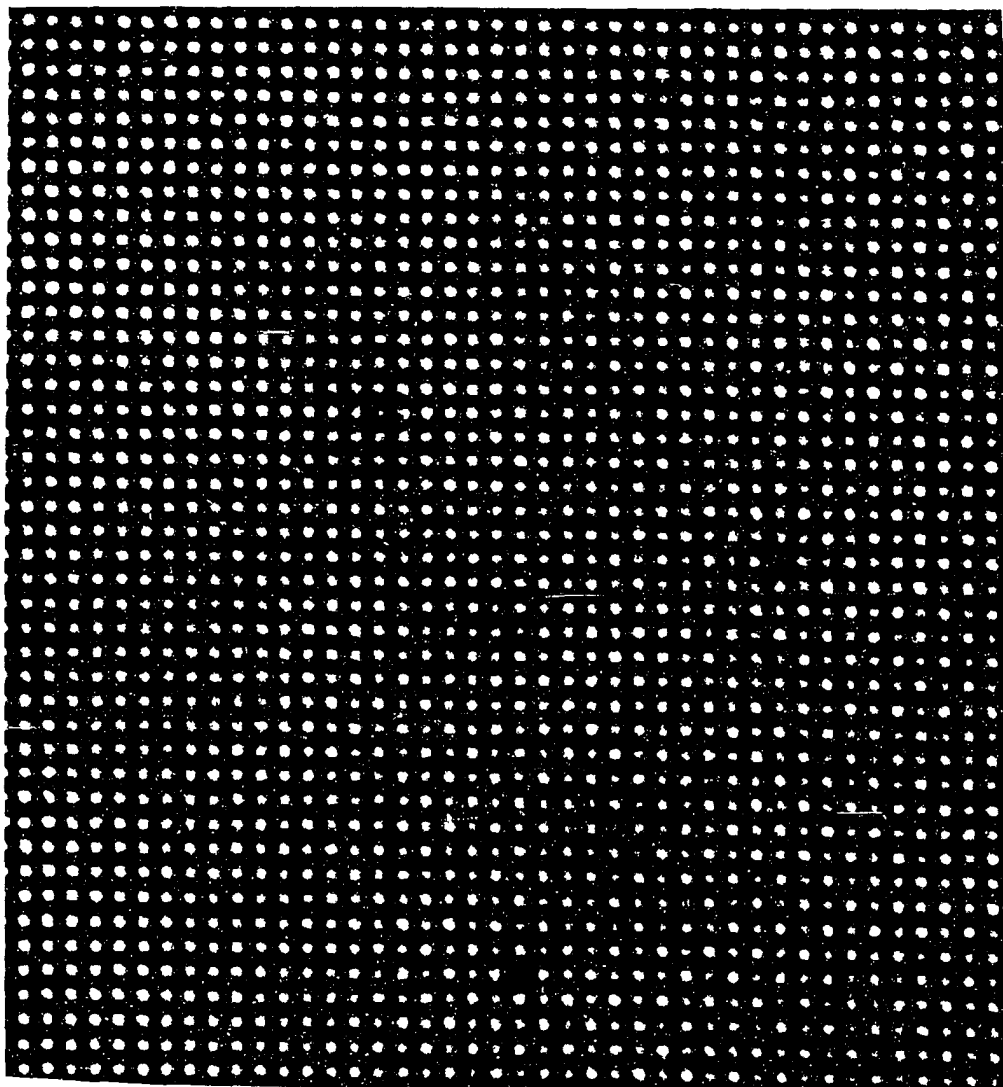
FIG. 3.18. Interference pattern at the edge of the Gaussian beam profile.
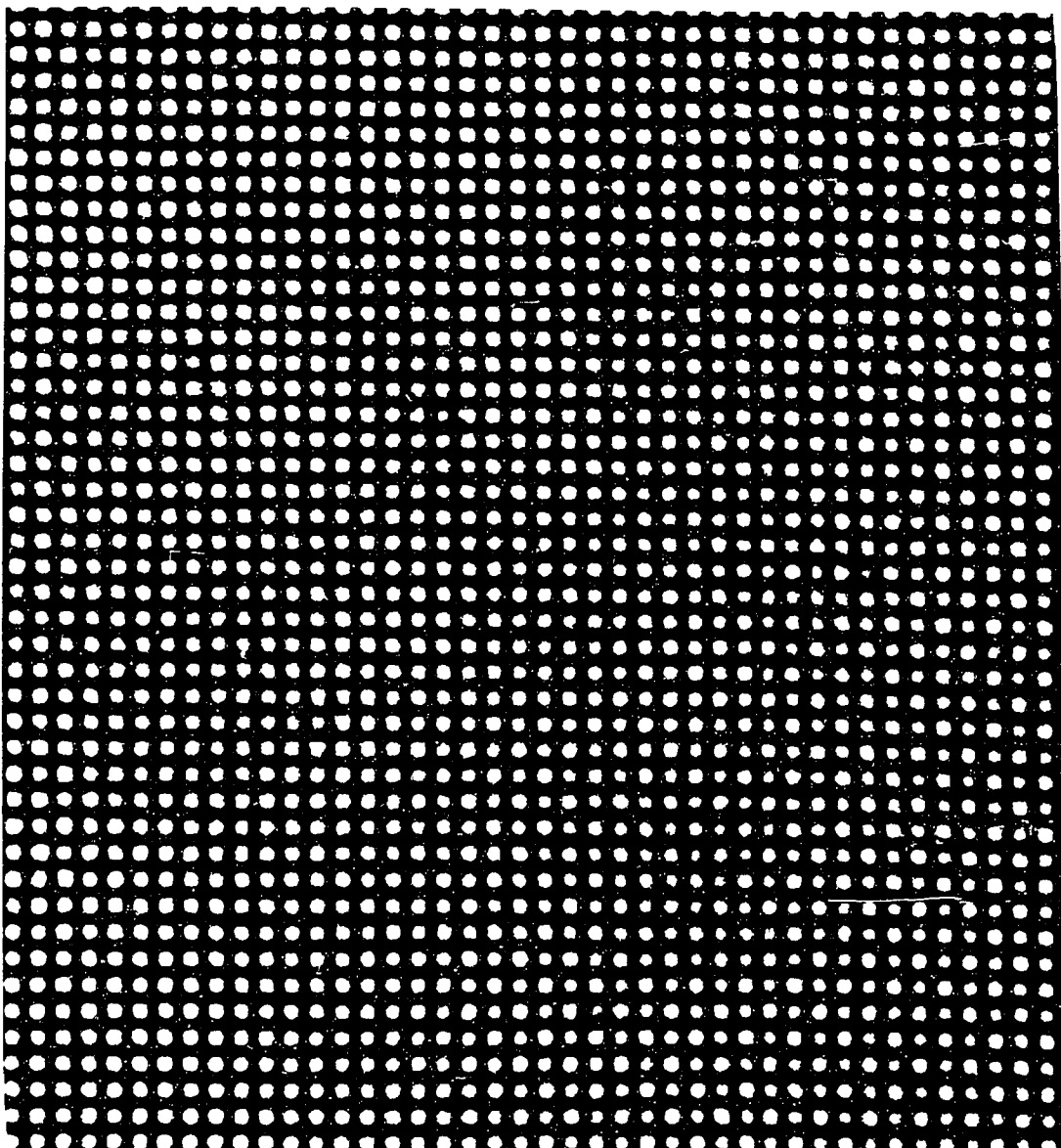
FIG. 3.19. Interference patterns at the center of the uniform beam profile.
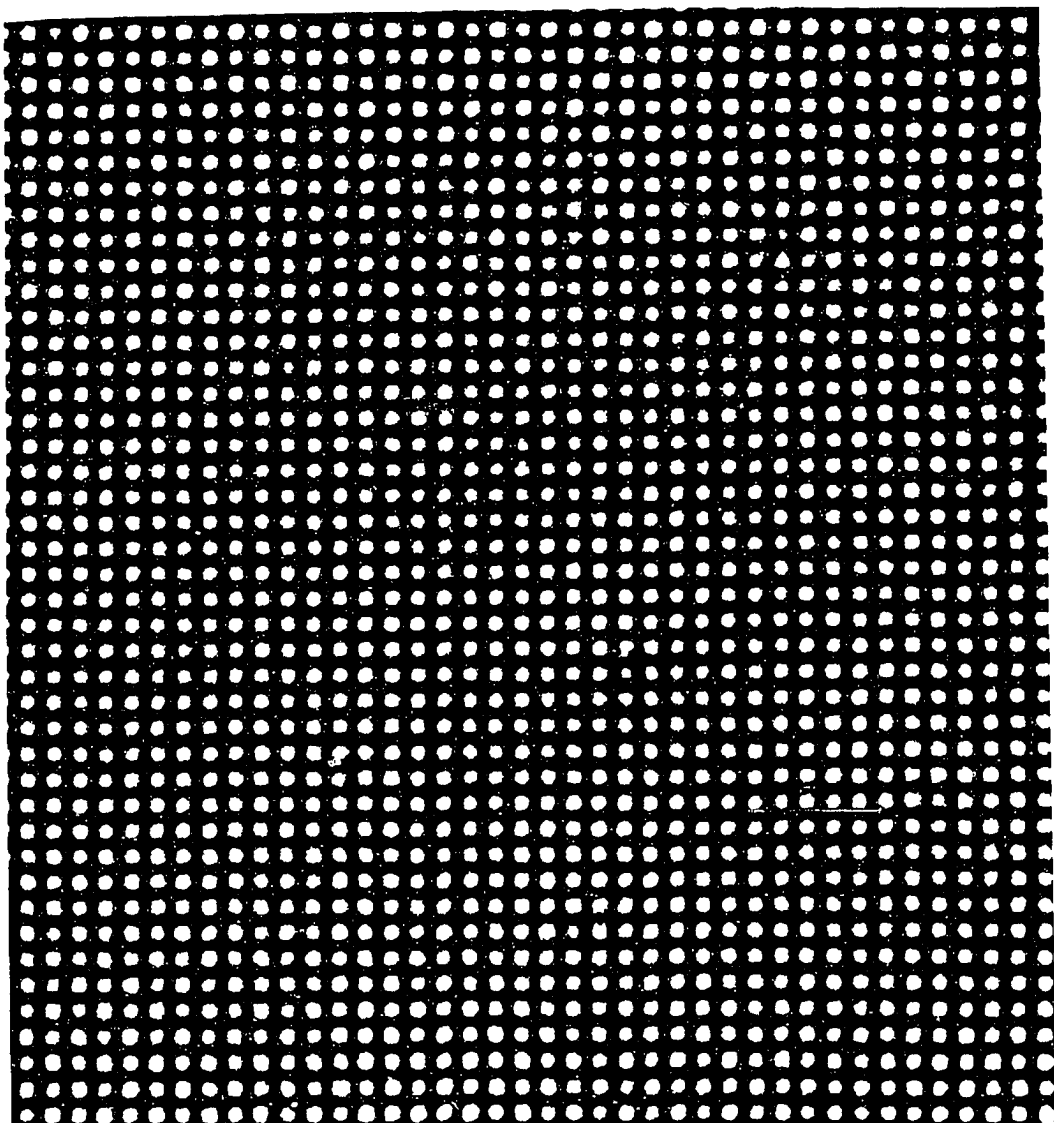
FIG. 3.20. Interference patterns at the edge of the uniform beam profile.

reshaping system enhanced the performance of the projection system, and this projector provided a whole new and unique method to produce directional light filters, optical arrays, and other micro-elements.

CHAPTER 4

CONCLUSIONS

The design and testing results of the beam profile reshaping system have demonstrated that a two-plano-aspherical lens system can effectively convert a radially symmetric beam profile into a uniform profile. In this study, an aspherical lens reshaping system was designed to convert a Gaussian beam into a uniform beam profile, and experimental results showed that such a refractive system is an energy efficient and simple beam profile reshaping system to build and test. Therefore, the design theory has been established. This reshaper was then integrated into a holographic projection system, which produces various interference patterns on film or photosensitive substrate to produce micro-optical arrays and directional light filters. Using the reshaper, the projection system can produce a full beam of uniformly illuminated interference patterns with maximum energy efficiency. Otherwise, the interference patterns will have maximum energy intensity at the center and will decrease at the edge, if a Gaussian beam profile is utilized. Variation in illumination creates severe problems controlling the exposure rates of various parts of a sample.

In this reshaping system, the aspherical surfaces of the two lenses are obtained by solving differential equations, which are established by the design conditions. Unlike the traditional optical design method, which optimizes the optical parameters to minimize a merit function, these differential equations are written to eliminate optical aberrations and conserve energy while reshaping the profile. Therefore, a system obtained from the solution of differential equations is an aberration-free system. Even through the differential equations may appear to be very complicated, they can be easily solved by

79

numerical methods. The numerical data of the surfaces then can be fitted by a conventional optical surface equation for future modelling and fabrication. Therefore, it was straightforward to manufacture these surface shapes using single-point diamond lathe cutting fixtures.

After design and analysis of the reshaping system, calculations have also been done to predict whether a beam reshaping system which is designed for a particular wavelength can be used to reshape a different wavelength of light. The computational results show that different wavelengths can be reshaped using one beam reshaper by simply varying the distance between the two aspherical lenses. The testing results of a HeNe laser (632.8 nm) beam profile by a reshaper, which was designed to reshape a HeCd laser (441.6 nm) beam profile, supported this prediction. This suggests that one reshaper can be used in different applications when different light wavelengths are required.

It is also very important to understand the required tolerances of the system parameters so that the beam profile will not be distorted by improper assembly. The investigation involved tilting and decentering the two aspherical lenses of this reshaping system. Testing results showed that this reshaper is a very stable system; however, the two lenses should not be tilted in opposite directions.

The promising results of the prototype of the beam reshaper system and the holographic projection system provide the motivation to design and fabricate a UV laser projection system as a production model in collaboration with Optimerix Company. This UV projection system is a revised and improved system of the prototype, and it will have a higher laser power and a larger beam size. It will be used to manufacture many kinds of micro-optical arrays and light filters.

With the increasing demand for laser illumination applications, such as laser projection systems, material processing, and laser fusion, it becomes very important to have a simple beam profile reshaping system with high energy efficiency. The two-plano-

aspherical lens system provides such a solution. Its application to the holographic projection system provides strong evidence that this refractive lens system will contribute to the advancement of uniform illumination applications in the future.

REFERENCES

1. B. Badger, H. A. Attaya, T. J. Bartel, M. L. Corradini, R. L. Engelstad, G. L. Kulcinski, E. G. Lovell, G. A. Moses, R. R. Peterson, M. E. Sawan, L. M. Goldman, R. E. Hopkins, L. D. Lund, R. L. McCrory, S. Skupsky, K. Walsh, "Preliminary conceptual design of SIRIUS, a symmetric illumination, direct drive laser fusion reactor," University of Wisconsin/LLE report on a direct-drive fusion reactor, (1984).

2. W. B. Veldkamp and C. J. Kastner, "Beam profile shaping for laser radars that use detector arrays," Appl. Opt. **21**, 345-356 (1982).

3. H. M. Haskal, "Laser recording with truncated Gaussian beams," Appl. Opt. **18**, 2143-2146 (1979).

4. P. W. Rhodes and D. L. Shealy, "Refractive optical systems for irradiance redistribution of collimated radiation: their design and analysis," Appl. Opt.**19**, 3545-3553 (1980).

5. D. Shafer, "Gaussian to flat-top intensity distributing lens," Opt. Laser Technol. **14**, 159-160 (1982).

6. J. W. Ogland, "Mirror system for uniform beam transformation in high-power annular lasers," Appl. Opt. **17**, 2917-2923 (1978).

7. P. W. Scott and W. H. Southwell, "Reflective optics for irradiance redistribution of laser beams: design," Appl. Opt. **20**, 1606-1610 (1981).

8. P. H. Malyak, "Two-mirror unobscured optical system for reshaping the irradiance distribution of a laser beam," Appl. Opt. **31**, 4377-4383 (1992).

9. W. B. Veldkamp, "Laser beam profile shaping with interlaced binary diffraction gratings," Appl. Opt. **21**, 3209-3212 (1982).

10. C. Y. Han, Y. Ishii and K. Murata, "Reshaping collimated laser beams with Gaussian profile to uniform profiles," Appl. Opt. **22**, 3644-3647 (1983).

11. C. C. Aleksoff, K. K. Ellis and B. D. Neagle, "Holographic conversion of a Gaussian beam to a near-field uniform beam," Opt. Egn. **30**, 537-543 (1991).

12. D. M. Dagenais, J. A. Woodroffe and Irving Itzkan, "Optical beam shaping of a high power laser for uniform target illumination," Appl. Opt. **24**, 671-675 (1985).

13. Y. Ozaki and K. Takamoto, "Cylindrical fly's eye lens for intensity redistribution of an excimer laser beam," Appl. Opt. **28**, 106-110 (1989).

14. U. Levy, "Diffractive optics spawns new products and a multimillion-dollar market," Photonics Spectra, 135-140, May, 1992.

15. C. Wang and D. L. Shealy, "Design of gradient-index lens systems for laser beam reshaping," Appl. Opt. **25**, 4763-4769, (1993).

16. W. Jiang and D. L. Shealy, "Optical analysis of the performance of a laser beam shaper," Sept. 1992. New Mexico

17. W. Jiang, "A refractive system for reshaping the irradiance distribution of laser beams," Dissertation proposal, Department of physics, UAB, December 1992.

18. W. Jiang, D. L. Shealy, and J. C. Martin, "Design and testing of a refractive reshaping system," Proc. SPIE, **2000-08**, San Diego, 1993

19. W. Jiang, D. L. Shealy and K. M. Baker, "Laser beam reshaping system used in holographic projectors," Seventh Annual Alabama Material Research Conference, Sept. 21-22, Normal, Alabama, paper B2-20.

20. W. Jiang, D. L. Shealy, and K. M. Baker, "Design and testing of a laser beam profile reshaping system," In Technical Digest on Materials Processing (Page 8) Toronto, Canada (Oct. 3-8), paper ME5.

21. K. M. Baker, D. L. Shealy and W. Jiang, "Holographic pattern generation with binary optics," In Technical Digest on Holography (Page 170), Toronto, Canada (Oct. 3-8), paper ThF6.

22. W. Jiang, D. L. Shealy and K. M. Baker, "Optical design and testing of a holographic projection system," Proc. SPIE, Los Angles, 1994, to appear.

23. K. M. Baker, D. L. Shealy, W. Jiang, "Directional light filter and monolithic microchannel array optical elements," to appear.

24. J. J. Cowan, "Method and apparatus for exposing photosensitive material," U.S.Pat. 4,496,216(1985)

25. J. J. Cowan, "The recording and large scale replication of crossed holographic grating arrays using multiple beam interferometry," Proc. SPIE **503**, 120-129, 1984.

26. J. J. Cowan, "The holographic honeycomb microlens," Proc. SPIE **523**, 251-259, 1985

27. T. Suzuki, K. Iizuka, K. Ohtaka, and H. Mizutani, "Focusing Plate," U. S. Pat. 4, 421,398 (1983)

28. D. L. Shealy and D. G. Burkhard, "Analytical illuminance calculation in a multi-interface optical system," Optica Acta **22**, 485-501 (1975).

29. Genesee Optics Software, 20 University Avenue, Rochester, NY 14605.

30. Melles Griot, Optics Guide **5**, 18-2.

31. Math/Library, "Fortran Subroutines for Mathematical Applications," IMSL Inc. Version 2.0, September, 1991.

32. Ealing electro-optics, Product Guide, K-13.

33. Handbook of Optics, page 7-83.

34. A. Meddler and R. Mead, "A simplex method for function minimization," Computer Journal, **7**, 308 (1965)

35. Principles of Optics, Max Born and Emil Wolf. Pergamon Press Inc. 1965.

36. Diffraction Gratings, M. C. Hutley. Academic Press, 1982.

37. Diffraction gratings as measuring scales, J. Guild, Oxford university Press, 1960

38. Scattering theory for diffraction gratings, Calvin H. Wilcox, Springer-Verlag, 1984.

39. Diffraction grating spectrographs, Sumner P. Davis, Holt, Rinehart and Winston, Inc, 1970.

40. W. B. Veldkamp, G. J. Swanson, and D. C. Shaver, "High efficiency binary lenses," Optics Communications, Vol 53(6), pp. 353-358.

41. Optics Guide 4, page 9-2.

42. Ken Baker, Optimerix, Inc. 13659 Victory Blvd, Van Nuys, CA 91401.

43. KLINGER catalog 584C, page 185.

44. Wayne Rasband, "NIH Image 1.44." It is a public domain image processing and analysis program for the Macintosh. It is available via anonymous FTP from zippy.nimh.nih.gov (128.231.98.32). The author also can be reached at wayne@helix.nih.gov.

APPENDIX A

THE OPTICAL DESIGN PROGRAM AND SUBROUTINES

```
C

C      ********************************************************

C      * THIS PROGRAM CALCULATES THE TWO SURFACES OF       *

C      * THE LASER BEAM RESHAPING SYSTEM NUMERICALLY       *

C      ********************************************************


C  THE BENEFITS OF THIS PROGRAM ARE

C      1. IT IS A VERY SIMPLE AND READABLE SHORT PROGRAM;

C      2. IT CAN CALCULATE ANY SIZE OF WORKING APARTURES;

C      3. ONLY FOUR NECESSARY PARAMETERS ARE REQUIRED;

C

C  HOW TO USE THIS PROGRAM

C      1. THIS IS A FORTRAN 77 PROGRAM, SO ITS NAME

C         SHOULD BE "FILENAME.F"

C      2. SINCE THIS PROGRAM USING SUBROUTINES OF IMSL,

C         ONE SHOULD USE "F77 FILENAME.F -LIMSL" TO

C         COMPILE AND LINK THIS PROGRAM

C

C      <Main Program>

       IMPLICIT REAL *8 (a-h,o-z)
       INTEGER NDEG,KORDER
       PARAMETER (NDEG=4)
```

85

```
      DIMENSION COEFF(NDEG+1)
      DOUBLE COMPLEX ZERO(NDEG)
      DEMENSION xpr(500),xsr(500),xx(500),yy(500)
      DIMENSION z1(500),z2(500),dzdr(500),ddzdr(500),ddzdr2(500)
      EXTERNAL DZPLRC,DQDAG,DDERIV,F,DZPLRC
      COMMON/INPUT/pr,sr,xn,xd


c     data pr,sr,xn,xd/0.8,1.25,1.43916,15.0/
      open(1,file='inten')
      open(2,file='r1z1')
      open(3,file='r2z2')
      open(4,file='spldat',form='formatted')

      write(6,600)
600   format('ENTER THE APERTURES AND INDEX FOR BOTH LENS',
      &/'AND THE DISTANT BETWEEN THE TWO LENSES')
      read(5,*) pr,sr,xn,xd


C     PR IS THE RADIUS OF WORKING APERTURE OF THE PRIMARY LENS,
C     AND SR IS THAT OF THE SECONDARY. XN IS THE INDEX FOR
C     BOTH LENSES, AND XD IS THE DISTANT BETWEEN THE TWO
C     VERTEXES OF THE TWO SURFACES. THE UNIT IS CENTERMETER.
C
      u=((1.0d0-dexp(-2.0d0))/2.0d0)*pr*pr/(sr*sr)
      write(1,*) u


C     u IS THE INTENSITY OF THE OUTGOING BEAM, AND THE
C     INTENSITY OF THE INCOMING BEAM IS UNIT

      do 10 i = 1, 100

      xpr(i) = float(i)*pr*0.1d-1

      xsr(i)=sr*dsqrt((1.d0-dexp(-2.0d0*(xpr(i)/pr)**2))
      &/(1.d0-dexp(-2.0d0)))

      xx(i) = xsr(i) - xpr(i)


C     xx(i) IS R-r
```

```
        yy(i) = (xn*(xn-1.d0)*xd+dsqrt((xd*(xn-1.d0))**2+(xn**2-1.d0)
     &*xx(i)**2))/(xn**2-1.d0)
```

```
C       yy(i) IS Z-z
```

```
        coeff(1) = xx(i)**2
        coeff(2) = 2.d0*xx(i)*yy(i)
        coeff(3) = (1.0d0-xn**2)*(xx(i)**2+yy(i)**2)
        coeff(4) = coeff(2)
        coeff(5) = -xn**2*(xx(i)**2+yy(i)**2)+yy(i)**2
```

```
        call dzplrc (ndeg, coeff, zero)
C
C       DZPLRC  CALCULATES  THE  ROOTS  OF  THE  FORTH  ORDER
C       POLYNOMIAL OF dz/dr
C
        do 20 j = 1,4
        if(DIMAG(zero(j)).NE.0.d0) go to 20
        if(DREAL(zero(j)).LT.0.d0) go to 20
        dzdr(i) = DREAL(zero(j))
20      continue
```

```
        errabs = .1d-14
        errrel = .1d-14
        a = 0.d0
        b = xpr(i)
```

```
        call dqdag(f,a,b,errabs,errrel,2,z1(i),errest)
```

```
        z2(i) = z1(i) + yy(i)
C
C       DQDAG CALCULATES THE INTEGRAL OF dz/dr. z1(i) IS THE z VALUE
C       AT r, AND z2(i) IS THE Z VALUE AT R. R RELATES r BY CONSERVATION
C       OF ENERGY, AND Z RELATES z BY CONSTANT OPTICAL PATH
C       LENGTH PRINCIPE
C
        bgstep = 0.1d-6
        tol = 0.1d-6
        korder = 1
        ddzdr(i) = dderiv(f,korder,b,bgstep,tol)
```

```
      ddzdr2(i)=ddzdr(i)*pr*pr/(2.0d0*sr*xpr(i))
     &*dexp(2.0d0*(xpr(i)/pr)**2)
     &*dsqrt((1.0d0-dexp(-2.0d0))
     &*(1.0d0-dexp(-2.0d0*(xpr(i)/pr)**2)))

      write(2,*) xpr(i),z1(i)
      write(3,*) xsr(i),z2(i)
      z1(i) = z1(i) + 0.5d0
      z2(i) = z2(i) + 0.5d0
      write(4,800) xpr(i),z1(i),dzdr(i),ddzdr(i)
      write(4,800) xsr(i),z2(i),dzdr(i),ddzdr2(i)
800   format(4(d22.15,1x))


10    continue


      close(1)
      close(2)
      close(3)
      close(4)

      stop
      end



      FUNCTION f(x)
      IMPLICIT REAL *8(a-h,o-z)
      INTEGER NDEG
      PARAMETER (NDEG=4)
      DIMENSION COEFF(NDEG+1)
      DOUBLE COMPLEX ZERO(NDEG)
      EXTERNAL DZPLRC
      COMMON/INPUT/pr,sr,xn,xd

      xsr=sr*dsqrt((1.d0-dexp(-2.0d0*(x/pr)**2))
      2/(1.d0-dexp(-2.0d0)))

      xx = xsr - x

      yy = (xn*(xn-1.d0)*xd+dsqrt((xd*(xn-1.d0))**2+(xn**2-1.d0)
```

```
      3*xx**2))/(xn**2-1.d0)

      coeff(1) = xx**2
      coeff(2) = 2.d0*xx*yy
      coeff(3) = (1.0d0-xn**2)*(xx**2+yy**2)
      coeff(4) = coeff(2)
      coeff(5) = -xn**2*(xx**2+yy**2)+yy**2

      call dzplrc (ndeg, coeff, zero)
C
C     DZPLRC CALCULATES THE ROOTS OF THE FORTH ORDER
C     POLYNOMIAL OF dz/dr
C
      do 20 j = 1,4
      if(DIMAG(zero(j)).NE.0.d0) go to 20
      if(DREAL(zero(j)).LT.0.d0) go to 20
      f = DREAL(zero(j))
20    continue

      return
      end
```

APPENDIX B

FITTING PROGRAMS FOR EXPERIMENTAL DATA

```
C
C    ***************************************************
C    * THESE PROGRAMS FIT THE EXPERIMETNAL DATA OF THE  *
C    * LASER BEAM PROFILE INTO A GAUSSIAN-LIKE FUNCTION *
C    ***************************************************


C  HOW TO USE THESE PROGRAMS
C     1. THESE ARE FORTRAN 77 PROGRAMS, SO THEIR NAMES
C        SHOULD BE "FILENAME.F"
C     2. ONE SHOULD USE "F77 FILENAME.F" TO
C        COMPILE AND LINK THESE PROGRAMS
C
C     <Main Program 1>
C     THIS PROGRAM CALCULATES THE SIGMA OF GAUSSIAN
C     DISTRIBUTION
      implicit double precision (a-h, o-z)
      parameter (npt=36)
      dimension r(npt),z(npt), fz(npt+1), r4(npt+1)

      open(2,file='the experimental data')
      open(3,file='value of sigma')
      r4(0)=0.d0
      fz(0) = 0.d0
      read(2,*) (r(i),z(i),i=1,npt)
```

```
         do 10 i=1, npt
         z(i) = dlog(z(i))
         r(i) = r(i)**2
         r4(i) = r(i)**2
         fz(i) = z(i)*r(i)
         fz(i) = fz(i-1) +fz(i)
         r4(i) = r4(i-1) + r4(i)
10       continue
         sigma = fz(npt)/r4(npt)
         sigma = dsqrt(-.5d0/sigma)
         write (3,*) sigma
         close (2)
         close (3)
         stop
         end
```

```
***************************************************************

C        <Main Program 2>

C        THIS PROGRAM CALCULATES THE NUMERICAL DATA OF THE

C        GAUSSIAN DISTRIBUTION


         implicit double precision (a-h,o-z)
         dimension gau(500)
         open(2, file='value of sigma')
         open(3,file='numerical data for the Gaussian distribution')
         read (2,*) sigma
         do 10 i = 17, 0, -1
         gau(i) = dexp(-0.5d0*(float(-i)/sigma)**2)
10       write(3,*) -i,gau(i)
         do 20 i = 1, 18
         gau(i) = dexp(-0.5d0*(float(-i)/segma)**2)
20       write(2,*) i,gau(i)
         close(2)
         close(3)
         stop
         end
```

APPENDIX C

CALCULATIONS FOR THE GRID SIZE OF THE INTERFERENCE PATTERNS

The grid size of the interference patterns of the prototype of this holographic projector can be obtained by ray tracing two rays which pass through the prisms system. These two rays should have optical path difference a half of the wavelength. The ray trace can be schematically shown as in FIG. C.1. According the calculations and the parameters given in sections 3.2.1 and 3.2.2, d_9, which is the distance between the two interference maxima, can be calculated.

5°
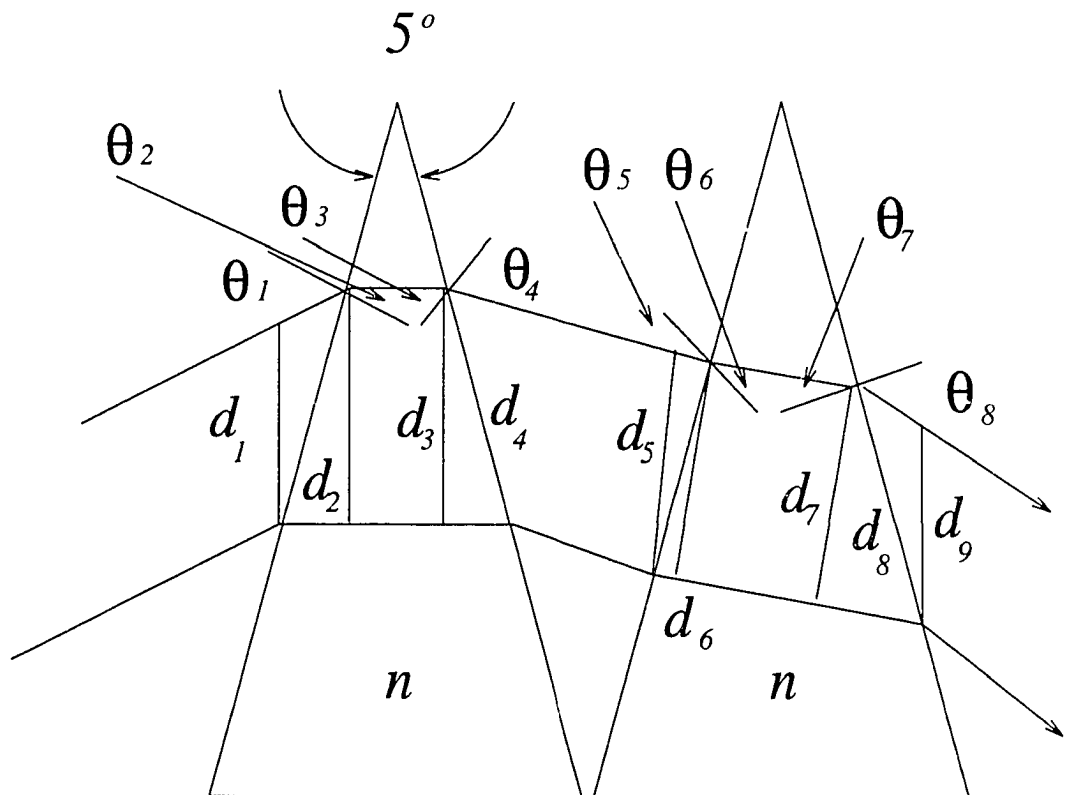
FIG. C.1. Ray trace of the two 5-degree prisms.

92

The angle θ_1 equals the diverging angle (section 3.1.2,) plus half of the prism angle, which is 2.5°. Then θ_2 can be calculated by Snell's law.

$$\sin\theta_1 = n\sin\theta_2, \tag{C.1}$$

$$\theta_2 = \left(\frac{\sin\theta_1}{n}\right)^{-1}. \tag{C.2}$$

$$\theta_3 = 180^0 - (180^0 - 5^0) - \theta_2 = 5^0 - \theta_2. \tag{C.3}$$

$$n\sin\theta_3 = \sin\theta_4, \tag{C.4}$$

$$\theta_4 = (n\sin\theta_3)^{-1}. \tag{C.5}$$

$$\theta_5 = 5^0 - \theta_4. \tag{C.6}$$

$$\theta_6 = \left(\frac{\sin\theta_5}{n}\right)^{-1}. \tag{C.7}$$

$$\theta_7 = 180^0 - (180^0 - 5^0) - \theta_6 = 5^0 - \theta_6. \tag{C.8}$$

$$\theta_8 = (n\sin\theta_7)^{-1}. \tag{C.9}$$

With these angles, the optical path difference for the two rays can be calculated as

$$d_2 = d_1\frac{\sin 91.226^0}{\sin(180^0 - 2.5^0 - 91.226^0)}. \tag{C.10}$$

$$d_3 = d_2\tan\theta_2. \tag{C.11}$$

$$d_4 = \frac{d_3}{\cos\theta_3}. \tag{C.12}$$

$$d_5 = d_4\cos\theta_4. \tag{C.13}$$

$$d_6 = \frac{d_5}{\cos\theta_5}. \tag{C.14}$$

$$d_7 = d_6\cos\theta_6. \tag{C.15}$$

$$d_8 = \frac{d_7}{\cos\theta_7}. \tag{C.16}$$

$$d_9 = d_8\frac{\sin(90^0 - \theta_8)}{\sin(180^0 - 2.5^0 - \theta_8)}. \tag{C.17}$$

The optical path difference is

$$\Delta_1 = d_3\tan\theta_2 + d_3\tan\theta_3 + d_7\tan\theta_6 + d_7\tan\theta_7. \tag{C.18}$$

$$\Delta_2 = d_1\frac{\sin 2.5^0}{\sin(90^0 - 2.5^0 - 1.266^0)} + d_4\sin\theta_4 + d_6\sin\theta_6 + d_7\frac{\sin 2.9^0}{\sin(90^0 - \theta_8)}. \tag{C.19}$$

$$\Delta = \Delta_1 - \Delta_2 = \frac{\lambda}{2}. \tag{C.20}$$

From Eq. C.20, d_9 was obtained. For, $n = 1.475$, and $\lambda = 441.57nm$, the distance between two maxima is approximately 25 microns.
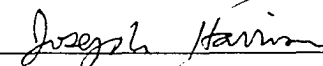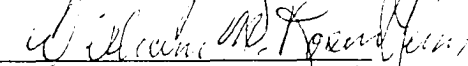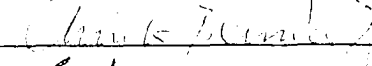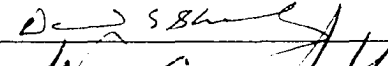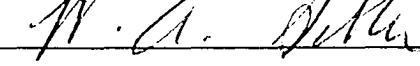
GRADUATE SCHOOL
UNIVERSITY OF ALABAMA AT BIRMINGHAM
DISSERTATION APPROVAL FORM

Name of Candidate _____ Wu Jiang _____

Major Subject _____ Physics _____

Title of Dissertation __Application of a Laser Beam Profile Reshaper to__

__Enhance Performance of Holographic Projection Systems_____

_____

_____

Dissertation Committee:

David Shealy _____ , Chairman _____

Joseph Harrison _____ _____

James Martin _____ _____

John Young _____ _____

Bill Rosenblum _____ _____

Christer Bennewitz _____ _____

Director of Graduate Program _____

Dean, UAB Graduate School _____

Date ____ 12/13/93 _____

PS-142B